Wright State University
CORE Scholar

Browse all Theses and Dissertations | Theses and Dissertations

2013

Effects of Red Diamondback Rattlesnake Venom on Keloid Dermal Fibroblasts *In Vitro*

Mackenzie Shelby Newman
Wright State University

Follow this and additional works at: https://corescholar.libraries.wright.edu/etd_all

 Part of the Pharmacology, Toxicology and Environmental Health Commons

Repository Citation

Newman, Mackenzie Shelby, "Effects of Red Diamondback Rattlesnake Venom on Keloid Dermal Fibroblasts *In Vitro*" (2013). *Browse all Theses and Dissertations*. 1164.
https://corescholar.libraries.wright.edu/etd_all/1164

This Thesis is brought to you for free and open access by the Theses and Dissertations at CORE Scholar. It has been accepted for inclusion in Browse all Theses and Dissertations by an authorized administrator of CORE Scholar. For more information, please contact library-corescholar@wright.edu.

Effects of Red Diamondback Rattlesnake Venom on Keloid Dermal Fibroblasts *In Vitro*

A thesis submitted in partial fulfillment of the
requirements for the degree of
Master of Science

By:

Mackenzie Shelby Newman

B.S., Miami University 2011

WRIGHT STATE UNIVERSITY

GRADUATE SCHOOL

10 January 2014

I HEREBY RECOMMEND THAT THE THESIS PREPARED UNDER MY SUPERVISION BY Mackenzie Newman ENTITLED Effects of Red Diamondback Rattlesnake Venom on Keloid Dermal Fibroblasts *In Vitro* BE ACCEPTED IN PARTIAL FULFILLMENT OF THE REQUIREMENTS FOR THE DEGREE OF Master of Science.

_____
Richard Simman, M.D., Thesis Director

_____
Norma C. Adragna, Ph.D.
Interim Chair, Department of Pharmacology and Toxicology

Committee on Final Examination

_____
Richard Simman, M.D.

_____
David Cool, Ph.D.

_____
Sharath Krishna, Ph.D.

_____
R. William Ayres, Ph.D.
Interim Chair, Graduate School

ABSTRACT

Newman, Mackenzie. M.S., Department of Pharmacology & Toxicology, Wright State University, 2013. Effects of Red Diamondback Rattlesnake Venom on Keloid Dermal Fibroblasts *In Vitro*

Keloid scarring is an inflammatory healing response to physical injury such as incision or piercing in the dermis. It is characterized by aberrant extracellular matrix production, the overaccumulation of mature collagen, and excessive fibroblast proliferation and migration beyond the borders of the original wound site. This results in swelling, depigmentation, itchiness, and pain akin to a benign tumor. Although there are myriad treatments for the condition, most are invasive and exhibit a high recurrence rate. Previous studies have shown that rattlesnake venom stimulates apoptosis in the skin via multiple specific mechanisms, largely composed of extracellular matrix and its receptors' interactions. The goal of this study is to isolate and identify constituents of *Crotalus ruber ruber* (*C.r.r.*) venom that may attenuate keloid fibroblast proliferation. Snake venom was ultrafiltered and fractionated on a cationic column in a fast protein liquid chromatography (FPLC) system followed by de-ionization through dialysis membranes. Normal fibroblasts and keloid samples were treated with fractionated venom and assayed for cell proliferation and collagen production, while venom was tested for its capacity to deplete collagen. Separated venom composition was described via MALDI-TOF and further qualified by specific activity studies. Our results suggest that *C.r.r.* venom contains novel peptides and may possess great therapeutic potential toward keloid scarring.

TABLE OF CONTENTS

LIST OF FIGURES Page

Page

LIST OF TABLES

LIST OF FREQUENTLY-USED ABBREVIATIONS

AU – Arbitrary units

C.r.r. – Crotalus ruber ruber

Da – Daltons

ddH2O – Deionized, distilled water

ECM – Extracellular matrix

FPLC — Fast protein liquid chromatography

KF – Keloid fibroblast

mL – Milliliters

MS – Mass spectrum

MWCO – Molecular Weight Cut Off

NF – Normal fibroblast

nm – nanometers

RDB – Red diamondback rattlesnake

TGFβ – Transforming Growth Factor-Beta

ACKNOWLEDGEMENTS

To Drs. DiFulvio, Grobe, Lauf, Sulentic, Brown, J. Miller, Adragna, Lucot, Elased, Chen, Lockwood, and Morris, thank you for showing me the ropes.

To Cathy Winslow, Laurie Schoettinger, and Stacy Gehret, thank you for helping me feel that I belong here.

To my labmates, classmates, and fellow researchers, thank you for being there.

To Venus, Amber, Kathryn, Rachel, Ekta, Bradley, Amanda Freeman, Prakash—I wouldn't have made it without you.

To my parents, Brenda and Marc, thank you for encouraging me to take the steps to get to where I am today, especially when I was stubborn and snarky. To my sisters, Alex and Carrie, thank you for your endless support.

To Richard Simman, Sharath Krishna, Billy Grunwald, Terry Oroszi, and David Cool, thank you for teaching me, letting me learn from you, and giving me this opportunity to mature.

This is for you, Uncle Bill.

BACKGROUND

Skin

The skin is an extremely complex organ that is the body's first defense against environmental factors. It is the largest organ of the human body with an average surface area of 1.5-2m^2 (Seifert, 2008). The integumentary system includes all layers of the skin, including the epidermis, dermis, and hypodermis. The epidermis is largely composed of keratinocytes, the dermis of fibroblasts, and the hypodermis of fibroblasts and macrophages. Varieties of specialized structures dwell in the skin, including hair follicles, sweat glands, and nerve terminals. The largest volume of the skin, the dermis, is composed mainly of extracellular matrix, i.e. collagens (Alberts, 2002), with a low degree of vascularization.

Wound Healing

Wound healing is one of the oldest studied biological processes (Bhatia, 2004). It is an immensely complex mechanism that involves myriad cell types and growth factors. It occurs in three or four principle, overlapping stages, depending on source; these may be limited to inflammation, proliferation, and maturation (Martin 1997; Broughton, 2006; Seifert, 2008).

During the first stage of wound healing, the primary goal of the injured tissue is to seal damaged blood vessels to attain hemostasis (Gousain, 2004). Clotting commences with the activation of platelets, primarily via the recognition of non-native collagens in the bloodstream (Nieuwenhuis, 1985) on integrin receptors (Jokinen, 2004). This leads to the

release of pluripotent cytokines such as transforming growth factor-beta (TGFβ), plateletactivating factor (PAF) (Parent, 1993), platelet-derived growth factor (PDGF) (Throckmorton, 1995) and vascular endothelial growth factor (VEGF) (Frank, 1995), and interleukin-1 (IL1) (Sauder, 1991). TGFβ primarily serves to induce production of extracellular matrix proteins and proteoglycans such as collagen, fibrin and fibronectin (Roberts, 1992). Platelet activating factor (PAF), a glycerophosphocholine ester, modulates leukocyte-driven platelet recruitment and degranulation (Topham, 1998). PDGF is a potent mitosis inducer that allows cells to skip the G1 restriction checkpoint in order to drive cellularity of the lesion that also attracts neutrophils and macrophages to the area (Diegelmann, 2004). IL1 promotes coagulation and helps stimulate the overall immune response (Sauder, 1991; Yang, 2012). Autocrine signaling in macrophages and neutrophils perpetuate the inflammatory phase of wound healing.

As leukocytes recede from the active wound, signals from wound-latent VEGF prime the site for angiogenesis for the second phase of wound healing (Romano, 2002; Bao, 2009; Wilgus, 2012). The stage, often dubbed "proliferation", lasts for up to two months after the initial injury. Fibroblast growth factors (FGF) such as FGF-2 and FGF-7 stimulate keratinocyte growth and migration (Yen, 2013) to stabilize the dermis with the outer layers of the epidermis; this process of reepithelization is mediated by mesenchymal cells and macrophages by autocrine TGFβ and paracrine epidermal growth factor (EGF) and tumor necrosis factor alpha (TNFα) (Chen, 2008). They work along with TGFβ, which is now secreted primarily by macrophages, neutrophils, and fibroblasts, to encourage collagen type III production in fibroblasts for the formation of granulation tissue to protect newly-formed blood vessels and bar infection-bearing microbes from entering the

wound site. More fibroblasts are generated by the actions of TGFβ and endothelin-1 on inactive fibrocytes to further produce matrix, matrix metalloproteases, and cytokines (Dawes, 1996; Reilkoff, 2011). FGFs and VEGF encourage endothelial cell growth and drive plasminogen activation (Mossesson, 2005).

The final phase of healing may take years to complete. It is known as "maturation" of the wound and is characterized as the terminal differentiation of the site. Tissue integrity may approach its original tensile capacity (Hoying, 2006; Demidova-Rice, 2012). Wounds contract while maturing due to the action of myofibroblasts in the area; these cells exhibit characteristics of muscle-derived fibroblasts and secrete large amounts of collagen-I while depleting stocks of granular collagen-III (Hoying, 2006; Demidova-Rice, 2012). PDGF and TGFβare major determinants in the progress of the maturation process that have been shown to directly affect the remodeling capacity of fibroblasts toward the production of structural matrix proteins such as collagen (Fujiwara, 2005) and laminin (Malinda, 2008; Stroncek, 2008), glycosaminoglycans including chondroitin and hyaluronan (Ellis, 1992; Hoffmann, 2012), matrix metalloproteases like MMP1 (collagenase) and MMP2 (gelatinase) (Fujiwara, 2005), and plasmin mediators such as plasminogen activator inhibitor-1 (PAI1), tissue urokinase (uPA), and kallikrein (Li, 2003; Kishibe, 2012). Tight regulation of the formation and degradation of the extracellular matrix is crucial during the maturation phase of wound healing for proper dermostasis

Scarring

Scarring is the final endpoint of wound healing. Scar tissue, which forms throughout the wound healing process, is constituted largely by fibrillar, cross-linked collagens,

especially mature, processed type I (Broughton, 2005).Scarring does not occur in human fetuses and other organisms with the appropriate regenerative capacity (Leung, 2012). The formation of scars has been correlated to wound duration (Vowden, 2011); because numerous ECM members are upregulated during healing, their overproduction is possible and reinforced by the prevalence of hypertrophic factors in disordered wound healing.

Keloid Phenotype

Keloid scarring is most often encountered as an overhealing response to dermal injury such as incision, piercing, or burning, though it has been observed to appear after itching, acne, spontaneously, and by other means (Seifert, 2008; Yi, 2013). Keloids appear more frequently in women than men by multiple accounts (Furtado, 2009; Gauglitz, 2011). All keloid scars are hypertrophic scars in nature, but not all hypertrophic scars are keloids (English, 1999); the ultimate characteristic of the subject is its capacity to recur after treatment or invade surrounding tissue (Simman, 2003; Fujiwara, 2005; Gauglitz, 2011). Children and elderly are less likely to form keloids than those aged 10-30 and non-white racial groups (Juckett, 2009). Some studies (Marneros, 2004; Nakashima, 2010; Zhu, 2013) that focus on families and individual racial groups profile genetic loci which may be of pharmacological interest reveal, for example, anEGF receptorchain and the ubiquitin ligase NEDD4. Keloids have been rated as having a considerable effect on

quality of life by those affected in multiple surveys (Bock, 2006; Furtado, 2009).

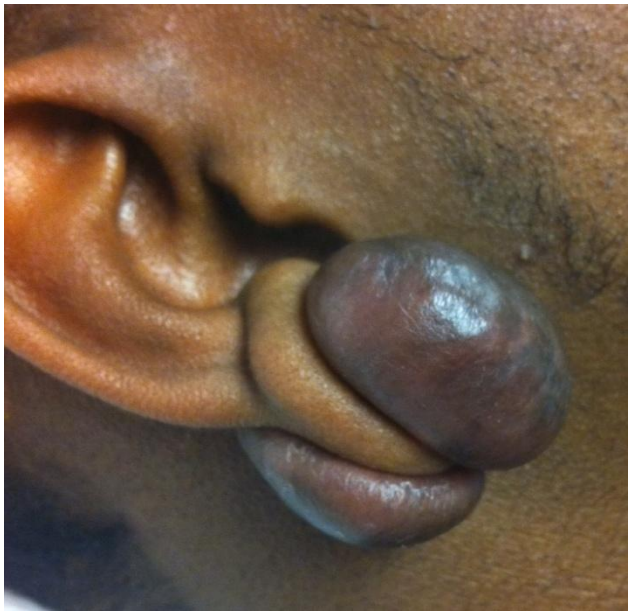

Figure 1: Male Earlobe Keloid Harvested for Study

Figure 1 is an example of an earlobe keloid that developed after the removal of ear gauages.

Keloid Pathology

Keloid scars have been exhibited to possess altered amounts of numerous chemical species, including but not limited to salts and small radicals (Chau, 2005; Ong, 2010) , glycosaminoglycans (Meyer, 2000) and glycoproteins (Babu, 1989; Chung, 2011), fats (Huang, 2013), oncogenic products (Saed, 1998; Russell, 2010), cytokines (Seifert, 2008), and, by definition, matrix proteins. Keloidal tissue is hypoxic (Kischer, 1992)and rather acellular compared to acute hypertrophic dermis (Moshref, 2010). It maintains more heavy metals and gelatins than normal skin (Bang, 2002) at least in part due to the enhanced production of matrix metalloproteases and ADAMs (Seifert, 2008; Imaizumi, 2009) , which simultaneously perpetuate the condition by encouraging cell migration and

fraying the matrix, therefore allowing mutant redifferentation. Sugar derivatives hyaluronic acid (Meyer, 2000; Seifert, 2008; Hoffmann, 2012) and fibronectin (Babu, 1989; Oliver, 1992) each have been a focus in keloids for their ubiquitous dysregulation in affected scars for their potential to normalize TGFβsecretion and slow cell migration due to significant interactions with cytokines, integrins, and ECM.

Keloids overexpress TGFβ. These scars are also commonly described with upregulated collagen-I (Chipev, 2000; Seifert, 2008), laminin (Lim, 2003), aggrecan (Shih, 2010), integrins (Szulgit, 2002),thrombins (Smith, 2008), plasmins (Tuan, 2003), and elastins (Smith, 2008). SMADs and matrix metalloproteases are dysregulated (Seifert, 2008). Excess collagens clump into amorphous semifibrillar granules that may intercalate other extra ECM molecules to promote disordered local adhesion. TGFβ-related pathways are overpromoted due to autocrine signaling in dermal fibroblasts that perpetuates ECM production (Chipev, 2000; Seifert, 2008; Bran, 2010).

Table 1: Differential Characteristics of Overgrown Scars (Seifert, 2008)

Keloids	Hypertrophic Scars
grow beyond the borders of the original wound	remain within the boundaries of the original wound
size varies between a peach and a football	size often only a few centimeters
pruritic and painful	less pruritic and painful
firm, erythematous nodule	firm, erythematous nodule
appear within several months after initial scar, then gradually proliferate indefinitely	generally arise within 4 weeks, grow intensely for several months, then regress often within one year
occur often on the chest, shoulders, upper back, back of the neck and earlobes, rarely on the palms or soles	no predominant anatomical site
do not regress spontaneously in general	generally regress spontaneously after the initial injury
larger, thicker and more wavy collagen fibres than normal skin, random collagen fibre orientation, increased ratio of type I to type III collagen	fine collagen fibres oriented parallel to the epidermis
increased fibroblast density and fibroblast proliferation rate	increased fibroblast density
only few α-smooth muscle actin expressing myofibroblasts	presence of α-smooth muscle actin expressing myofibroblasts is typical

Keloid Fibroblasts

Keloid fibroblasts are considered to be the progenitors of keloid scar pathology (Seifert, 2008). Previous research has shown them to show markers of numerous cell types, including but not limited to osteocytes (Naitoh, 2005), keratinocytes (Felice, 2007), endothelial cells (Seifert, 2008), chondroblasts (Inui, 2011), chondrocytes (Naitoh, 2005), and myofibroblasts (Chipev, 2000; Seifert, 2008). These mutants appear primarily at the margins of scars where the lesion is spreading; fibroblasts isolated from the centers of keloid scars have been shown to be characteristically normal (Lu, 2007). Compared to plain hypertrophic fibroblasts, keloidals are larger and fewer in population (Seifert,

2008). Both their cytoplasmic space and nuclei appear to be engorged compared to normal fibroblasts. Whereas normal fibroblasts are spindle-shaped with some arm-like projections, keloids express many acute, long, and non-arrayed appendages (Yi, 2013). Keloid fibroblasts may develop from senescent cells in the dermis or surrounding tissues; isolated cells exhibit a larger capacity to migrate and invade versus normal fibroblasts (Fujiwara, 2005).

TGFβ Signaling

Transforming growth factor-beta (TGFβ) is a cytokine that is involved in numerous cellular process including cell cycle regulation, differentiation, apoptosis, endosome formation and degradation, and embryonic development (Kanehisa, 2000; Kanehisa, 2014). It is one of the most promulgated molecules implicated in keloid pathology (Babu, 1992; Seifert, 2008). TGFβis upregulated in nearly all tissues normally but is especially present in kidney, lung, bone, and placenta (Branton, 1999). It has been shown to predominate in numerous fibrosis-related disorders, including liver cirrhosis, atrial fibrillation, pulmonary fibrosis, and keloid scarring (Ueha, 2012). The identification of TGFβ is attributed to Anita Roberts (Sporn, n.d.). The peptide is classified as an activin analogue due to its affinity for activin receptors; type I TGFβreceptorsaredescribed as "activin-like kinase 5" or ALK5 (Nicolas, 2003; The Uniprot Consortium, 2013). Since its initial isolation, TGFβhas become the titular constituent of a superfamily of proteins which all contain a similar cystine superstructure. Some of the key members of this group include nodal, activin, and bone morphogenic proteins which are implicit in neuronal and embryonic homeostasis (Wu, 2009). The eight reduced cysteines are connected in a "cysteine knot" pattern while the ninth is covalently bonded to another TGFβ monomer

(Daopin, 1992).

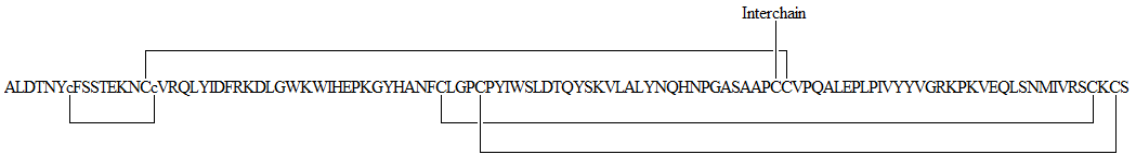

Figure 2: TGFβ Quaternary Structure ("C" is cysteine; capitalization denotes conserved cystine in TGFβ superfamily) (Hart, 2003; The Uniprot Consortium, 2013)

TGFβ is secreted is a propeptide into the extracellular space as a 390 residue-long chain that is cleaved to yield the active, 112-residue TGFβ monomer. After cleavage, TGFβ remains associated to its zymogen core, then known as latency associated peptide (LAP). The latency complex remains dormant and may be further coordinated by latent-transforming growth factor beta-binding protein 1 (LTBP1) to prevent receptor binding. When complexed TGFβ is activated, for example by matrix metalloproteases, it binds a type II receptor dimer which phosphorylates a type I receptor dimer at a serine residue. Activation of a type I receptor leads to SMAD disengagement from the receptor in the cytoplasm and gene transcription downstream that allows the production of extracellular matrix proteins (Roberts, 1998).

Integrin Signaling

Integrins are integral membrane proteins that are a cell's primary sensors of the extracellular matrix. They play a role in adherence, mechanotransduction, motility, cell shape, and regulation of the cell cycle (Kanehisa, 2000; Kanehisa, 2014). The surface receptor is typically encountered a heterodimer of at least one alpha and one beta integrin subunit while the internal receptor exists as the association of a variety of proteins and peptides(Brinkerhoff, 2005). A third of all integrins contain an RGD (or similar, such as

MVD or KGE) recognition motif that binds sites on collagens and fibronectin to establish stable matrix fixation (Barczyk, 2009). Large phosphorylated complexes known as "focal adhesions" constitute stable integrin receptors. Detachment and dissolution of focal adhesions results in anoikis, a specialized form a cell death related to matrix interaction (Frisch, 2001). Integrins bind ECM molecules such as collagen, laminin, fibrinogen, and vitronectin directly (Barczyk, 2001). They also play a vital role in hemostasis; integrin αIIbβ3, also known as glycoprotein receptor αIIbβ3, is expressed ubiquitously on platelets and allows them to form a thrombus. This property has become the subject of medical intervention in recent years (Bledzka, 2013).

Modern Treatments

Scars have been treated with a gamut of medicines throughout history. The most frequent initial treatment for keloid scars today is corticosteroid injection. Excision is a common secondary treatment but may be avoided due to the prevalence of recurrence associated with it. Chemotherapy drugs, radiation therapy, silicone gel sheeting, cryosurgery, and experimental therapeutics appear often in literature as alternative remedies (Simman, 2003; Juckett, 2009; Hunasgi, 2013). One relevant clinical trial recorded the effects of bacterial collagenase injected into keloid scars; all patients suffered from gross necrotic lesions (Kang, 2006). Others focus on the use of unsaturated fatty acids, including those derived from snake oil, to reduce scarring (Datubo-Brown, 1990); historical, anecdotal evidence both supports and dissuades the legitimacy of the use of snake oil as a scar remedy (Louw, 2000; Louw, 2006). Among all the scar treatments described in the literature, all are far from perfect with respect to disease recurrence (Simman, 2003; Juckett, 2009; Hunasgi, 2013).

Snake Venom

Snake venom is a mixture of proteins and peptides that are evolutionarily targeted toward the capture and digestion of prey. It is produced exclusively in a modified salivary gland and is secreted through a specialized ductal-fang delivery system to be delivered to its target. The proteomic components in snake venom exhibit a plethora of biological activities, such as anticoagulation (Bledzka, 2013), extracellular matrix cleavage (Teixeira, 2005), hemorrhage (Mori, 1987a), platelet activation (Bledzka, 2013), thrombus dissolution (Morais-Zani, 2009), angiogenic stimulation (Masaki, 1998), mitosis via growth factors (Momic, 2011), cell membrane disruption (Mayer, 1993; Rádis-Baptista, 2011), generation of peroxide (Torii, 1997), ion channel disfigurement (Dutertre, 2010), and DNA breakdown (Dhananjaya, 2010), and ATP depletion (Kini, 1982). Snake venom also contains numerous short peptides, nucleic acid derivatives, and organic compounds that are purported to function as inhibitors of the enzymes in venom, including but not limited to tripeptides (Munekiyo, 2004), nucleotides and nucleosides, and citrate (Mackessy, 2009).

All snakes have a common ancestor. The evolution of venom composition is tightly connected to the prey of the snake. Similarly, as snakes age, the size of prey correlates to that of the predator. Snakes dwell in nearly all habitats across the planet, with the exception of arctic regions. All snake venoms contain highly targeted neurotoxins, cytotoxins, myotoxins, and hemotoxins. Most of the toxins the produce the former three functions act non-enzymatically. Neurotoxic venom components target acetylcholinergic synapses and ion channels, while cytotoxins and myotoxins bind ion channels, transporters, and carriers that are typically present in heart, neural, and muscle tissue.

Hemotoxic venom components are often encountered as enzymes that lyse blood components and prevent proper thrombus formation in wound healing (Mackessy, 2009).

Snake Venom Therapeutics

Snake venom is an ideal focus for therapeutics because it is targeted toward mammalian tissue. Research into the uses of venom began, largely, in the 1970s and 1980s, with a surge in development of rapid proteomic screening tools including FPLC and HPLC. One of the initial snake venom derivatives to make it to market in the United States was captopril, an early ACE inhibitor (Smith, 2003). It was developed using QSAR in a similar fashion to tirofiban, another venom drug and the first to be designed through this mode. Tirofiban is an anticoagulant that binds platelet integrin αIIbβ3 (Bledzka, 2013). Eptifibatide, a cyclopeptide based on southeastern pygmy rattlesnake venom, exhibits the same mechanism of action (Bledzka, 2013). Three high-profile proteases from snake venom that have been investigated for use in the United States include ancrod (Lowe, 1982), batroxobin (Hao, 2012), and fibrolase (Markland, 2010). Each is described for its affinity to cleave fibrinogen and its ability to produce a blood clot; these drugs are implemented as anticoagulants when interference cannot be encountered in platelet signaling. Study endpoints for the first two were met and the drugs are marketed today; the third could not pass phase III trials for peripheral arterial occlusion and central venous accession. Other venom components have been explored in biological systems for therapeutic potential (Jain, 2010; Kurozumi, 2012; Marangoni, 2013) but none have made it past phase III trials in the United States.

Red Diamondback Snake & Venom

Table 2: Snake Venom Peptides (Harvey, 2006; Mackessy, 2009)

Protease Inhibitor Homologs	Three-Finger Toxins
Enzyme Inhibitors	α-Neurotoxins
Dendrotoxins	Muscarinic Toxins
Ca^{2+} Channel Blockers	Anticholinesterases
Crotamine-Like Myotoxins	Three-Finger, Disintegrin-Like
Sarafotoxins	Ca^{2+} Channel Blockers
CRiSP family	Cardiotoxins
Natriuretic Peptides	Synergistic Toxins
Disintegrins	
C-type Lectins and Lectin-like	Others
Waglerins	Phospholipase A2 (active and non-active)
Bradykinin-Potentiating Peptides	Growth Factors (VEGF, NGF)
AVIT Peptides	Hyaluronidase
	Snake Venom Metalloprotease

Crotalus ruber ruber, colloquially "red diamondback rattlesnake", is the nominate subspecies of rattlesnake that is indigenous to the southwestern United States and northern Mexico (Straight, 1992). It is a considerably long snake that is characterized as producing large volumes of venom (Mackessy, 1985). This red-hued rattlesnake's venom shares many characteristics of that of *Crotalus* spp. including sharp proteolytic activity and ECM-binding properties (Mackessy, 1985; Mori, 1987a; Hamako, 2007). It is considered to produce weaker biological reactions than that of many other rattlesnakes (Hamako, 2007; Komori, 2011), but this property is compensated in nature by the snake's large size which allows more venom to be delivered. Proteolytic activity in venom is typically higher in adults and snakes in captivity (Mackessy, 2009; Komori, 2011).

Table 3: Previously Identified Proteins and Peptides in *Crotalus ruber* Venoms (Mackessy, 1985; Mori, 1987a; Mori, 1987b; Takeya, 1990; Straight, 1992; Takeya, 1993; Hamako, 2007; Komori, 2011; Carey, 2012)

Protein Name/Family	MW	pI	# AA	Sequence?
Phosphodiesterase	98000	10.5	886	No
HT-1*	60000	5.8	216	Yes
R ester hydrolase E1	32000	5.2	290	No
R ester hydrolase E2	33000	4.6	291	No
Kallikrein-like enzyme	31000	4.6	271	No
HT-3	25500	9.6	257	No
Rubelase	24000	9.2	248	Yes
HT-2 (Ruberlysin)	24000	5.2	248	Yes
C-type Lectin	15000	5.3	135	Yes
Rubistatin (cloned)	6400	6	61	Yes

*Data varies per source

The venom of *Crotalus ruber* subspecies has been assayed for numerous properties and many proteins and peptides have been sequenced; a summary of these is provided in Table 3. Notably, a report by Mackessy describes L-amino acid oxidase activity in *C.r.r.* venom and evidence from our laboratory and other crotalid sequences suggests that at least one unsequenced protein similar to apoxin-I exists in *C.r.r.* venom.

Ruberlysin

A major constituent of *C.r.r.* venom is ruberlysin, a zinc- and calcium-dependent SVMP characterized as inducing hemolysis and necrosis in experimental settings. Ruberlysin is a mildly acidic ~23,321Da protein. It shares homology and identity with many human matrix metalloprotease, ADAM (A disintegrin and metalloprotease), and ADAMTS (ADAM with thrombospondin motifs) gene products (Altschul, 1990). Residues 153-155 of ruberlysin are KGD (Komori, 2011; The Uniprot Consortium, 2013) which functionally act like a traditional RGD motif to bind collagens, integrins, and other ECM effector molecules.

Table 4: Specific Cleavages of Various Substrates by Ruberlysin (Schomburg, 2013)

Peptide	Cleavage Site
Angiotensin I	Asp-Arg-Val-Tyr-Ile-His-//-Pro-//-Phe-His-Leu
Fibrinogen	α-Chain (not β- or γ-)
Insulin B Chain	...His_{10}-//-Leu-Val-Glu-Ala-//-Leu-Tyr-//-Leu-Val_{18}...
	...Cys_{19}-Gly-Glu-Arg-Gly-//-Phe-Phe-Tyr_{26}...
LHRH	pGlu-His-Trp-//-Ser-Tyr-Gly-//-Leu-Arg-Pro-Gly-NH2
Met-Enkephalin	Tyr-Gly-Gly-//-Phe-Met-NH2

The malleability of the active site of ruberlysin is revealed by various studies on the specific activity of ruberlysin-containing fractions of snake venom: this SVMP appears to possess both hydrogen-bonding and nonpolar binding affinity sectors; see Table 4 for details. Ruberlysin was initially denoted as HT-2 by Stephen P. Mackessy for the median MW fraction determined by SDS-PAGE. This toxin, along with HT-1 and HT-3, resolved as one of the venom's three major peak-fractions after HPLC and gel filtration by absorbance intensity at 280nm (Mackessy, 1985). All fractions possessed hemorrhagic properties and the first two have been sequenced (Takeya, 1990; Takeya, 1993). There is some disagreement about the N-terminus of ruberlysin: one source reports glutamine (The Uniprot Consortium, 2013) in the sequence while another reports a post-translation-modified form, pyroglutamate (Takeya, 1990). A second, modified ruberlysin-like SVMP has been sequenced and characterized from *C.r.r.*; rubelase differs from ruberlysin by four amino acids but was much less potent toward hemorrhage induction (Komori, 2011).

Hypothesis

The most prominent keloid characteristics are collagen accumulation and production and increased fibroblast lifespan. Rattlesnake venom is comprised of a number of proteins and components that normally act synergistically to produce the desired effect in its prey. Venom components that bind and/or cleave collagens and/or ECM constituents are likely to directly influence the pathways associated with the proliferation of keloid fibroplasias. Rattlesnake venom has been shown to stimulate apoptosis in myriad cell types via a variety of cell-specific mechanisms. These mechanisms include but are not limited to interactions with the ECM and its receptors, ion carrier disturbance, and membrane disruption. Due to the unknown nature of the constituents of *C.r.r.* venom on keloid fibroblasts, it is necessary to characterize these proteins and peptides and their relevant properties in order to sieve toward a disease treatment.

The hypothesis is that the separation and identification of these whole venom constituents by mechanical means will allow a more detailed analysis of the potential of specific components for therapeutic use. Additionally, the application of these *Crotalus ruber ruber* venom components to keloid dermal fibroblasts will elicit more pronounced effects to phenotypic and proliferative properties compared to those of normal human dermal fibroblasts.

Specific Aim 1

Develop a working scheme to isolate single proteins and peptides from red diamondback venom.

Specific Aim 2

Evaluate the ability of separated *C.r.r.* venom to cause proliferation or death on keloid scar and normal dermal fibroblasts.

Specific Aim 3

Determine the efficacy of separated venom components at reducing keloid fibroblast phenotypic characteristics such as collagen production.

Specific Aim 4

Identify proteins and peptides from fractionated snake venom.

II. MATERIALS AND METHODS

1. Venom Collection

Crotalus ruber ruber venom was manually procured in the laboratory of animal research at Wright State University every two weeks. The snake was fed at the end of each two-week period and its terrarium was tended between venom collections. Two sterile Eppendorf tubes were covered with fresh parafilm and aligned in front of a red diamondback snake's fangs. The snake handler, Dr. Sharath Krishna, held the snake from behind its head and teased it into secreting venom into the containers by waving a sacrificed mouse in front of its face. The collected product was quickly transported to Central State University on ice, lyophilized overnight, and stored at -20ºC until further use.

2. Venom Rectification

Desiccated, frozen venom (around 10mg) was dissolved in one milliliter of distilled, deionized water (ddH2O) using a Millipore Academic Milli-Q system. For some experiments, this was rectified into filtrates and insolubles through 10K, 30K, or 50K molecular weight cutoff filters (Millipore, catalogue UFC501024 (10K), UFC503024 (30K), UFC505024 (50K)) before FPLC treatment. The resultant solutions were processed using a Bio-Rad DuoFlow FPLC System which employed 100mM tris(hydroxymethyl)aminomethane (Tris) (A) and 100mM Tris plus 500mM NaCl (B) as buffers, each adjusted to pH 7.6 using concentrated hydrochloric acid. After sample injection, 1.8mL of (A) was run at 3mL/minute before a linear gradient was applied

between the buffers for 13mL at 4mL/minute. At the same rate, isocratic flow was resumed with 100% (B) for 10.8mL and then 100% (A) for 15mL at the end of the process. Thirty one-milliliter fractions were collected in total.

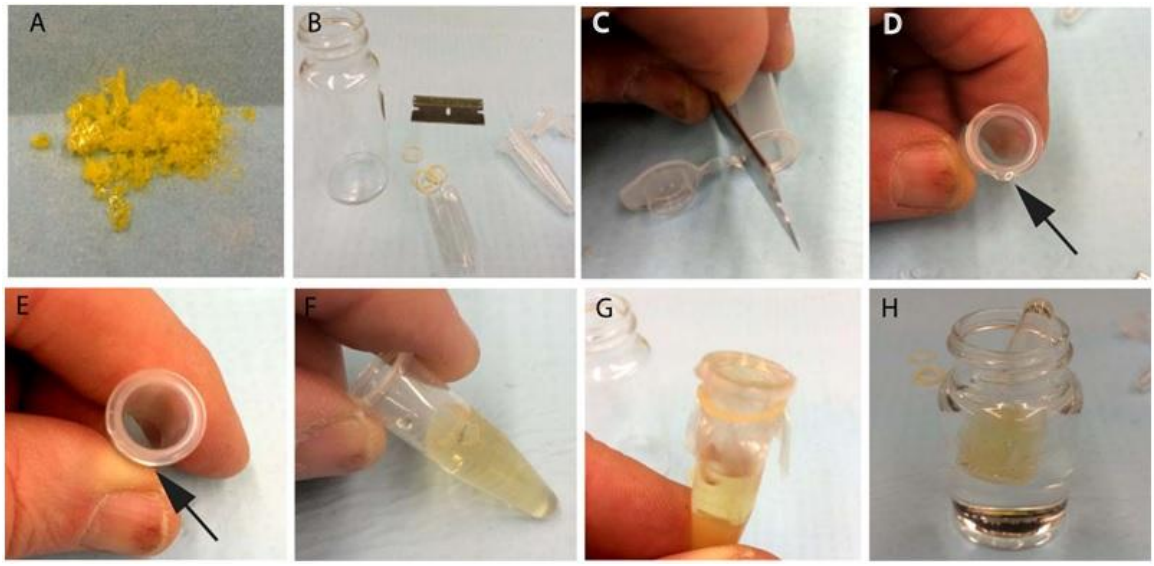

Figure 3: Apparatus for Venom Dialysis

Figure 3 displays the methodology used for venom dialysis: the lids, including hinges, were removed from 1.5mL microfuge tubes with a razor blade (Figure 3C), making sure to smooth the edge of the tube tops (Figure 3D and Figure 3E). The fractions which possessed significant absorbance at 214nm were immediately transferred into these microfuge tubes. Cellulose dialysis membrane ("Spectra/Por6" 1kD MWCO, Spectrum Labs, catalogue 132636) was sectioned, stretched over the top of each tube (Figure 3F), and secured around the edge with 5/16" elastic bands (Figure 3G). The tubes were then inverted to test for leaks and placed into individual vials of deionized, distilled water (Figure 3H). The dialyzing units were allowed to stand for one hour in order fully equilibrate solute gradients before the water was exchanged; this was repeated four times.

The de-salted venom fractions were then deposited into 1.5mL microfuge tubes and frozen at -20ºC for future experiments.

3. Identification of Venom Components

3.1 Whole Fraction Digestion

The protocols for Sigma product T6567 were adapted for these procedures. Fifteen microliters of 50mM ammonium bicarbonate solution were mixed with 1.5µL of 100mM dithiothreitol in a 0.5µL microfuge tube and followed by 25µL of venom fraction. The mixture was reduced at 95ºC for five minutes in a water bath while 100mM iodoacetamide was prepared in a foil-wrapped tube. Three microliters of the latter were added to the cooled samples and incubated in the dark at room temperature for 20 minutes. Trypsin stock was prepared at a concentration of 0.1g/L from proteomics grade porcine pancreatic trypsin (Sigma, catalogue T6567) and two microliters were added to each tube. Samples were digested overnight at 30ºC and immediately processed by the protocols described in 3.3.1.

3.2 Component Digestion

3.2.1 SDS-PAGE Electrophoresis

Twenty microliters of Laemmli sample buffer 2X (Bio-Rad, catalogue 161-0737) with five percent 2-mercaptoethanol were added to 20µL of sample and this was boiled in a 0.5mL microfuge tube for five minutes. The then-darkened samples were allowed to cool to room temperature and all forty microliters were pipetted into 4-20% Tris-HCl gels (Bio-Rad, catalogue 345-0032). Protein stacking was observed for twenty minutes at 100V and separation was performed at 180V for forty-five minutes. After ceasing the applied voltage, the gel was carefully removed from the electrophoresis chamber and

placed in a clean blotting box on an undulating shaker. It was gently swirled with 25mL of deionized, distilled water for five minutes, fluid was pipetted from the box, and then the proteins were fixed with 25mL of a 50% acetic acid/7% methanol solution for fifteen minutes. Fixing solution was discarded and the remnants were washed away with three five-minute interval water exchanges. The gel was then stained for 45 minutes using GelCode Blue Safe Protein Stain (Thermo Scientific, catalogue 24594) and excess stain was washed away by another set of water exchanges. Resolute bands from the finalized gel were selected and cut out with a razor for further processing. These individual bands were used immediately in the methodology described in 3.2.2 or stored overnight at 20ºC.

3.2.2 In-Gel Digestion

The methods of Shevchenko et al. (2007) were adapted for these procedures. Ammonium bicarbonate at a 50mM concentration (C) was used to prepare stock buffers of 25mM ammonium bicarbonate (D) and 1:1 50mM acetonitrile (ACN)/ammonium bicarbonate (E). One hundred microliter aliquots of (C) were added to tubes containing the stained protein bands from 3.2.1 and let stand for 10 minutes. Supernatant was discarded before 50µL of (E) was added and drawn off twice in ten-minute intervals. The gel band was dried in a centrifugal evaporator for five minutes while 10mM dithiothreitol was dissolved into (D). This solution was added in 20µL lots to the tubes and samples were heated at 37ºC for 60 minutes. Fresh 55mM iodoacetamide was prepped in (D) then added in 20µL quantities to the cooled samples. Incubation in the dark was permitted for 45 minutes at 37ºC. After the tubes reached room temperature, 100µL of (D) were used to wash the gel for 10 minutes. The fluid was sucked away before 100µL of (E) was inserted and taken away for ten minutes two times. Samples were vacuum centrifuged for five

minutes to ensure full dehydration of the gel disk. Sequencing grade trypsin was brought to a 20mg/L density in (D). Fifteen microliters were added to each tube along with 15µL of (D). Samples were digested overnight at 37ºC. Fluid was then removed after centrifugation, 20µL of 0.3% trifluoroacetic acid (TFA) was pipetted directly onto the gel band, and three extractions were performed with a 50% ACN/0.3% TFA mixture for ten minutes each. The volume of the collected supernatant was reduced to 10µL via vacuum centrifuge. The final samples were stored at -20ºC until processed by the protocols of 3.3.1.

3.3. Mass Spectrometry

3.3.1 Protein Preparation

The resultant peptide mixtures from 3.1 and 3.2.2 were prepared for mass spectrometry using C18 ZipTips (Millipore, catalogue ZTC18M096). A series of five 1.5mL tubes was prepared for each sample including one of pure acetonitrile, two of 0.1% TFA, one with 95% ACN/0.3%TFA, and an empty tube for sample collection. ZipTip procedures by Amanda Freeman were then followed directly. After purification, unknown samples were mixed 1:1 with 10mg/mL CHCA and 1µL was spotted onto a 384-well ground steel plate.

3.3.2 MALDI-TOF Parameters

A Bruker Daltronics Autoflex III Smartbeam MALDI-TOF mass spectrometer was used in conjunction with components of the Autoflex software (including Flexcontrol, Flexanalysis, and Biotools) to obtain all mass spectrometry data. The system was calibrated with Peptide Standards II (Bruker Daltronics), omitting data points with an error rate greater than $0.015Da^{-1}$, before each use. Default method protocols for MS and MS/MS measurement were used with no alteration. Laser intensity was set around 80%

for MS collection, 90% for parent ion identification, and 100% for protein fragmentation. Data were passed through the MASCOT and Swissprot database servers set exclusively to search metazoan datasets against a monoisotopic distribution with two or fewer partial (missed) cleavages, potential oxidation at methionine residues as the sole variable modification, a mass tolerance of 400ppm, an MS/MS tolerance of 1.0Da, and a charge state of +1. Peaks of interest were selected from the derived spectra using the Bruker SNAP processing parameter algorithm with a signal-to-noise threshold of 6 and quality factor threshold of 50.

4. Peptide Cleavage Assay

Buffers and substrate concentrations suggested in the description for Sigma product F5135 were used as guidelines for these experiments. FALGPA (N-[3-(2-Furylacryloyl)]-L-leucyl-glycyl-L-prolyl-L-alanine) (Crescent Chemical Company, catalogue 51565.01) was dissolved at 5μg/mL and 1μL was added with 1μL of 0.36mM calcium chloride and 50mM HEPES at pH 7.0 to 10μL of each snake venom fraction. Aliquots of the reactions were placed in sealed Eppendorf tubes in a 37ºC dark incubator for 45 minutes. Reactions directly spotted for MALDI-TOF using standard CHCA matrix.

5. *In Vitro* Studies

5.1 Cell Isolation and Expansion

Wright State University IRB SC#4833was written and filed for these experiments. Dermal samples were acquired from the earlobe ofa consenting African American male, age 24, under care in the private office of Dr. Richard Simman. KF1 cell line was cultured by Dan Yi by the following protocol:

"Skin specimens were first washed with phosphate-buffered saline (PBS) (Gibco, Life Technologies™, USA) three times to exclude erythrocytes, then cut into 2.5mm x 2.5mm pieces and incubated with 2ml digestion medium containing high glucose Dulbecco's Modified Eagle's Medium (DMEM) (Gibco, Life Technologies™, USA),5 mg/mL collagenase/dispase II (RocheDignotics, USA) and 0.25% trypsin (Invitrogen, Life Technologies™, USA) in 60x15mm tissue culture dish for 8h at the condition of 5% CO_2, at 37°C.Then the tissue suspension was passed through a 100 mm filter (BiologixResearch Company, USA) to remove any remaining tissue residuals. The suspension was next centrifuged at 300 G for 8 min to obtain cell pellet. This pellet was transferred to a T25 cell culture flask cultured with 3 ml total medium containing high glucose DMEM, 10%FBS (Gibco, Life Technologies™,USA),1% Pen/Strep/Glutamine (Invitrogen, Life Technologies™, USA) in the condition of 5% CO_2, at 37°C. Cells took approximately 3 days to totally attach to the bottom and reach to confluence in about 10 days. After cells were attached the bottom of the flask, total medium was replaced with fresh total medium. During cell growth, every 2 or 3 days medium was changed after PBS washing to exclude the flatting dead cells. Once reaching confluence (named as Passage 1) cells were detached into a new passage by 0.05% trypsin (Invitrogen, LifeTechnologies™, USA)." [sic] (Yi, 2013)

Normal fibroblasts (NF) were cultured from frozen samples of isolated cells from dermal tissue of an African American female of similar age to the primary specimen. Keloid fibroblast cells, derived from a 35-year-old African American female, referred to as KF2, were purchased from ATCC (product CRL-1762). They were notably late-generation (at passage 11) and marked as having doubled in population at least ten times since initial

storage at the company. All fibroblast cell lines were maintained in routine culture using DMEM modified with glucose (4.5g/L), glutamine, and antibiotics (streptamycin, amphotericin, and penicillin). Consecutive cultures were passaged with 0.25% trypsin (Mediatech Cellgro, catalogue 25-050-Cl) using untreated DMEM for washing and full media for quenching. Incubation followed standard protocol of 5% CO_2 and 37ºC exposure in darkness.

5.2 Fibroblast Proliferation Assays

NF, KF1, KF2, and cells were raised to ~80% confluency in T75 flasks before trypsinization and plating with nystatin-containing complete DMEM into 8-well chamber slides. Five slides of each cell type were prepared and allowed to reach full confluency or slightly overgrow in order to ensure appropriate cell quorum for microscopy. Media was replaced with 150μL previously-prepared venom dilutions in serum-free DMEM (1e-6 original concentration) and the slides were covered and incubated for six hours at 37ºC under 5% CO_2.

5.3 MTT Assay

Normal fibroblasts were incubated overnight in 96-well plates at a cell density on the order of 1e5 cells/mL. All reagents were prepared from a stock kit ("TACS(R) MTT Cell Proliferation Assays", Trevigen, catalogue 4890-50-K). Snake venom stock was prepared at one-half original concentration in DMEM and a 1:10 serial dilution of this was made down to 1e-7 the initial stock. Media was aliquoted to each well to adjust to a total volume of 150uL/well after venom addition. Plain media was used as a control. After 3 hours' exposure and incubation, 10uL MTT reagent was added and allowed to react in a

dark cell culture incubator for three hours. After noting the appearance of purple coloring in the wells, the plates were removed from the incubator and left overnight in the dark at room temperature. Plates were read in a plate reader for their absorbance at 535nm.

5.4 Collagen Integrity Assay

The methods of Walsh et al. (1992) were modified for these protocols. Cells were plated in 96-well microplates with lids and allowed to settle overnight in complete media. Serial filtered venom fractions were prepared at 1e-6 their original concentrations in DMEM and applied to cells after removing original media. After four hours' incubation at 37ºC under 5% CO_2, the plates were immediately placed in a-20ºC freezer and well contents were allowed to solidify overnight. The following morning, lids were removed and the plates were wrapped loosely in foil and left overnight in a dry incubator at 37ºC. Wells were rinsed three times for one-minute increments with 200µL of distilled water. Picrosirius red dye was prepared by the addition of Direct Red 80 (Sigma, catalogue 365548) to saturated picric acid solution at a 0.1% (w/v) concentration and 100µL was added to each well for one hour. The wells were rinsed five times with 200µL of 10mM HCl at 10 seconds per exposure and then 200µL of 0.1M NaOH for 5 minutes. The stained collagen slurry was gently mixed ten times up and down in a pipettor and transferred to a new plate for absorbance measurement under a 535nm filter.

5.5.1 van Gieson Staining

The methods of Ellis (2013) and Hunasqi (2013) were modified for these experiments. Hoescht 33258 was diluted from stock, hemotoxylin was used directly from stock, and Curtis' stain was made from 9:1:1 saturated picric acid: glacial acetic acid: 1% Ponceau

S. Nuclei were first bound by Hoescht for 90 minutes and then hemotoxylin was applied for five minutes. After, Curtis' stain was applied for five minutes to stain collagens. All dyes were aliquoted into 150μL volumes for each sample and reactions were carried out at 37ºC, under CO_2, in the dark. All wells were carefully rinsed between stains with ddH2O until no color appeared to leach into solution.

5.5.2 Microscopy

After the final histological solution was flushed, 4% paraformaldehyde was added to each well for 30 minutes at 4ºC. The chambers were then removed from the slides and each was rinsed in ddH2O. Fluorogel with Tris buffer (Electron Microscopy Sciences, catalogue 17985-10) was applied to coverslips which were immediately affixed to the slides. A Leica DMR B microscope operated with Leica TASv3.7 software was employed for all microscopy. Due to physical restrictions, differentiation between Ponceau S and picrosirius dyes was not detectable so photographs were recorded only for Hoescht and picrosirius.

5.6 Quantitative Proliferation Assay

All cell lines were individually seeded in 96-well plates in duplicate for the following procedures. Fibroblasts were allowed to grow past full confluency in order to ensure appropriate population and matrix density and encourage mild senescence as present in keloidal tissues. Venom fractions at 1e-6 the original concentration in plain media were applied in 100µL aliquots to fibroblast cells for four hours in duplicate. After removing the treated media and rinsing the wells twice with ddH2O, propidium iodide (10µg/mL) was applied for thirty minutes in the dark at room temperature. Plates were read in a Packard Fusion microplate reader for fluorescence using an excitation filter at 600nm and an emission at 620nm.

III. RESULTS

Develop a strategy to mechanically separate proteins and peptides from red diamondback venom

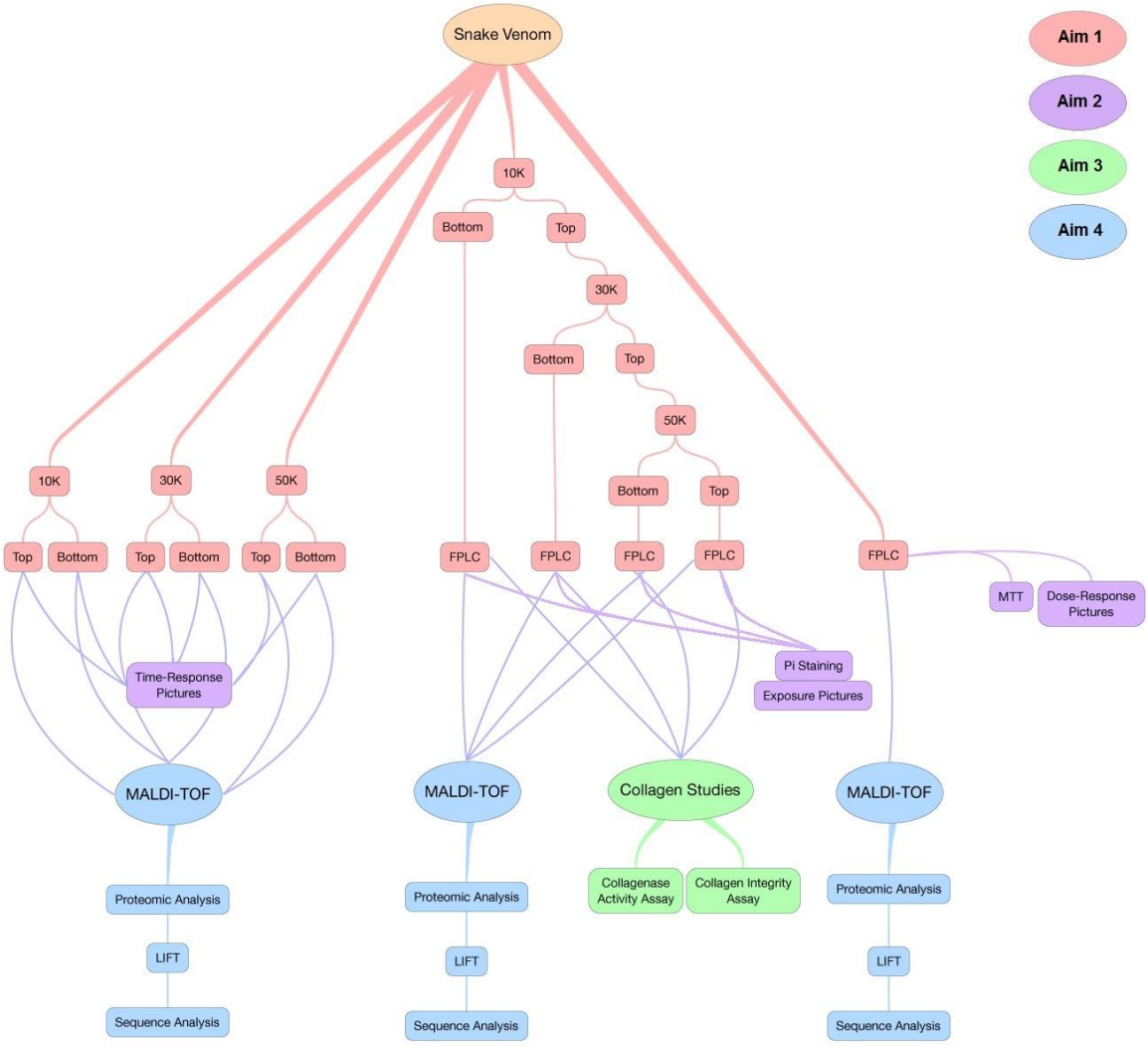

Figure 4: Workflow for Experiments

The workflow used for all experiments is displayed in Figure 4. After separation treatments (red; Aim 1), venom was tested for cell responses (purple; Aim 2), collagen-related effects (green; Aim 3), and for peptide and protein sequencing (blue; Aim 4).

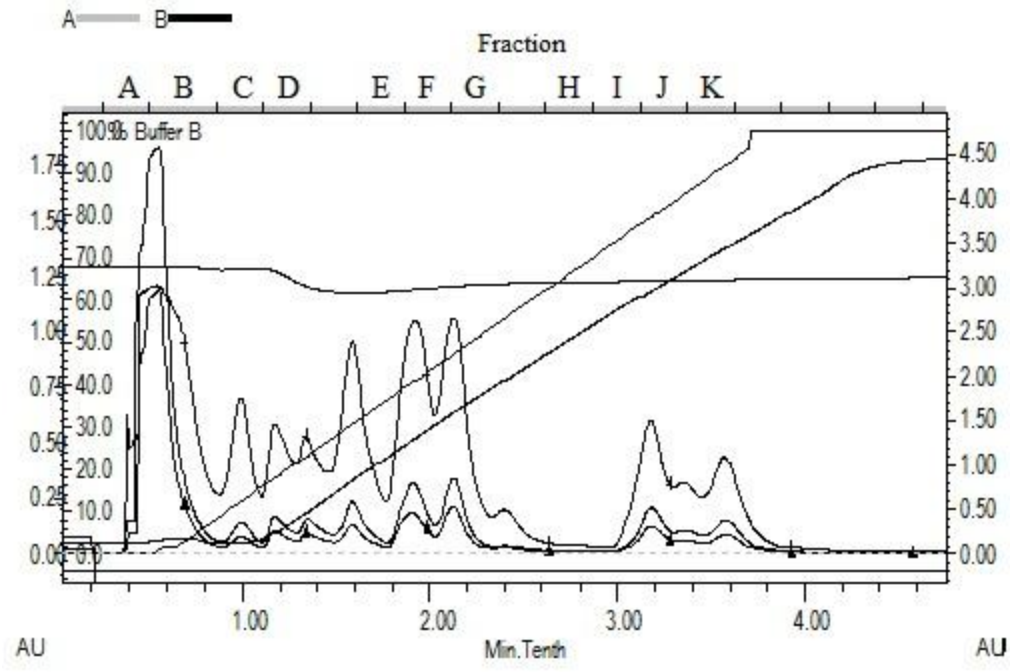

Figure 5: FPLC Output after Injection of RDB Venom

Figure 5 shows the absorbance of the FPLC effluent at 214nm, an indicator of peptide bond concentration, and the fractions chosen for further testing. Fractions exhibiting resolute peaks in noticeable concentration were selected. Fractions F, G, J, and K each contain at least two defined peaks.

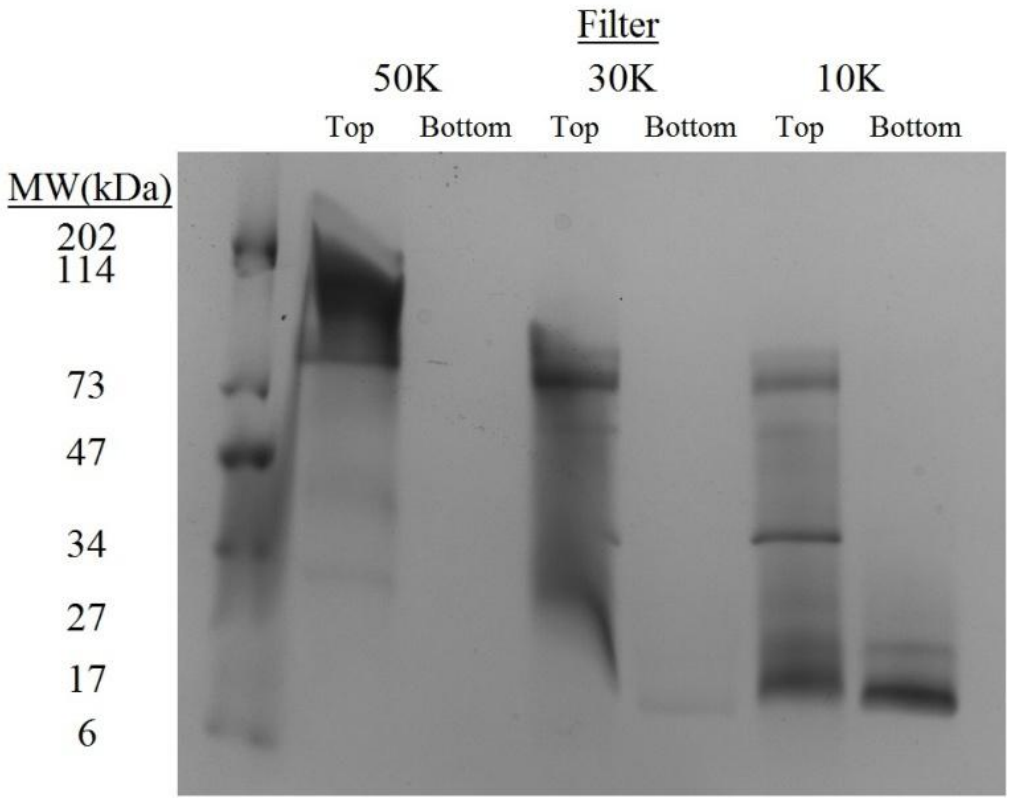

Figure 6: SDS-PAGE Gel of 10K, 30K, and 50K Filtered Venom

Figure 6 is an SDS-PAGE separation of RDB venom after the application of different MWCO filters. RDB venom distilled into resolute classes of peptides. The band around 17kDa is most likely a hemorrhagic toxin, based on early protein gel recovery experiments (data not shown). The dark band present in both the 50K and 30K filter tops was unidentifiable via mass spectrometry but suspected to but some form of HT3 given its size class.

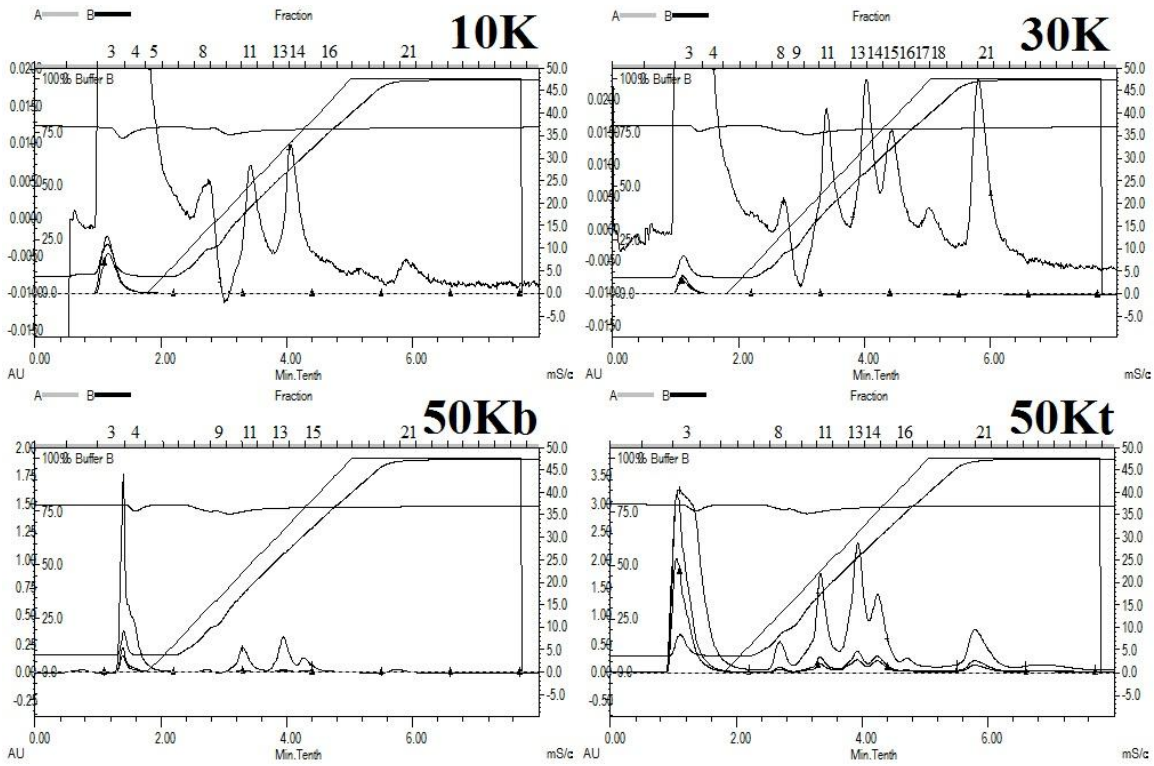

Figure 7: FPLC Output for Venom Separated via Serial Filtration

Figure 7 shows the FPLC outputs for each post-filtration venom separation. The injection peaks (the first major peak) in the 10K and 30K diagrams have been scaled out of the picture in order to accent the differences in the minor peaks. Separation is not visible given the height of the injection peak. Differential absorbance at 214nm (AU; displayed on y-axis) was observed in all processes.

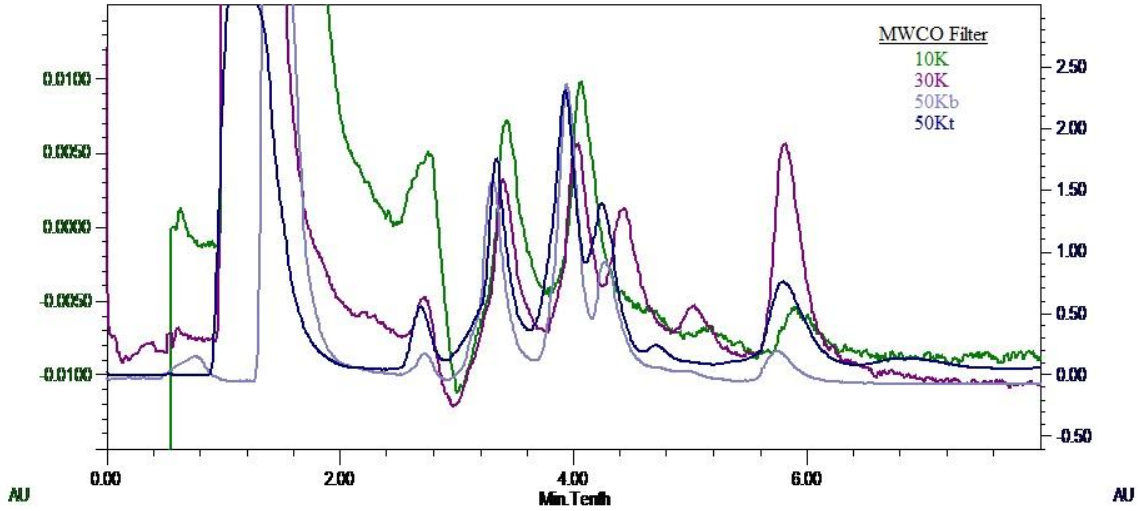

Figure 8: Composite of FPLC Output of Venom Separated via Serial Filtration

Figure 8 shows the relative quantitative protein distribution about the samples passed through the FPLC. A similar pattern of amplitudes is present in all runs but the distribution of prominent intensities varies per filtration, implying that different products are concentrated at different points throughout the filtration process. The height of the injection peak (the first major peak, truncated in the figure due to size constraints) changes considerably between the samples due to reduced venom density after successive filtration; this may have a considerable effect on the resolution of the measured spectra.

Evaluate the ability of separated *C.r.r.* venom to cause proliferation or inhibition on keloid scar and normal dermal fibroblasts

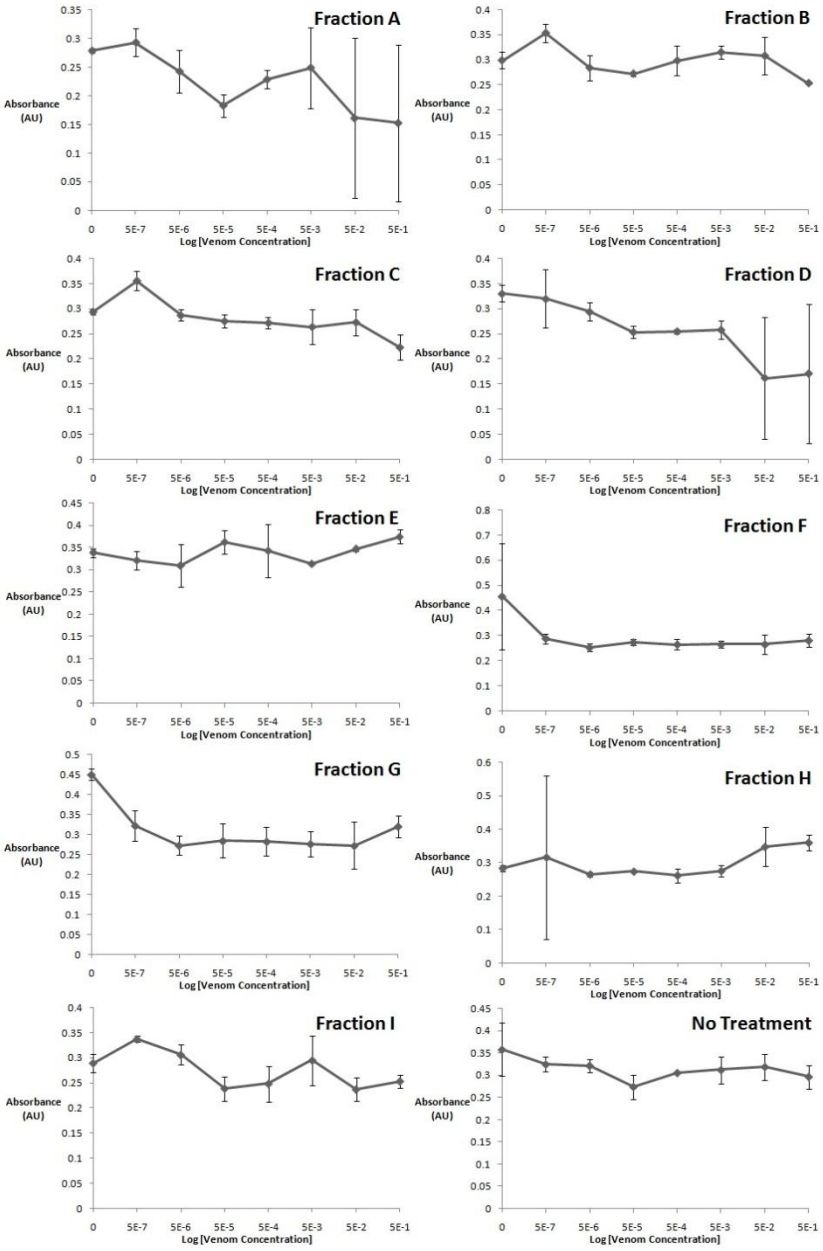

Figure 9: Spectrophotometric Absorbance of MTT Dye at 535nm after Serial Dilution Venom Exposure at Three Hours

MTT assay is a measure of cell viability: the dye is a bulky, sterically-hindered, optically-active and reactive molecule that shifts from visible yellow to purple upon reduction. The

results from serial venom dilution exposures, displayed in Figure 9, suggest a mixed response from fibroblast cells. The untreated group showed a similar response in all lanes. Color change implying inhibition of cells or the induction of oxidoreductive signaling—an overall trend downward—was observed in fractions A, C, D, F, and G. The last two fractions showed sharp responses at the lowest doses used. Proliferation was suggested by the absorbances recorded from exposure to fraction H. Fractions B, E, and I exhibited scattered effects. A difference in one aberrant point from each of these datasets would cause an overall sloping trend to appear more consistent.

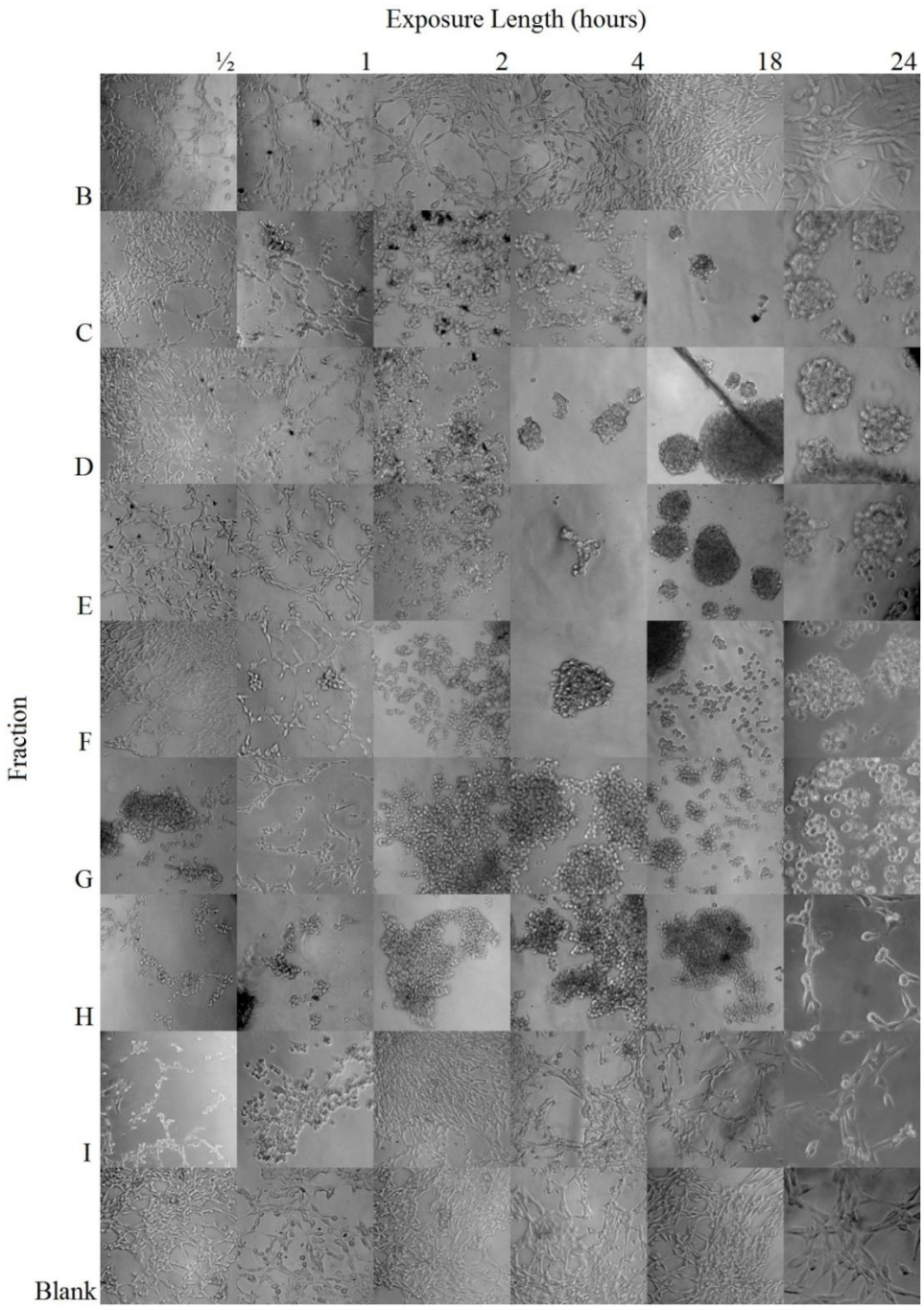

Figure 10: Normal Fibroblasts Exposed to Venom at Various Concentrations over a 1-Day Period

Enzyme contamination is evidenced by the effect of the venom fractions depicted in Figure 10: numerous fibroblasts were observed to be floating after treatment, their

spindle-like arms were degraded along with broad surface features of intact ECM, and acellular debris was accounted at numerous time points in each fraction. Fraction 2 possessed little visible activity, while fractions 3 through 7 caused noticeable fibroblast detachment and degradation within one hour. Fractions 8 and 9 displayed lytic activity but some recovery was noted at the end of the 24-hour exposure period; after one day of treatment, the cells appeared to clump and regenerate their arms. Similar effects were noted in the other active fractions but to a reduced degree.

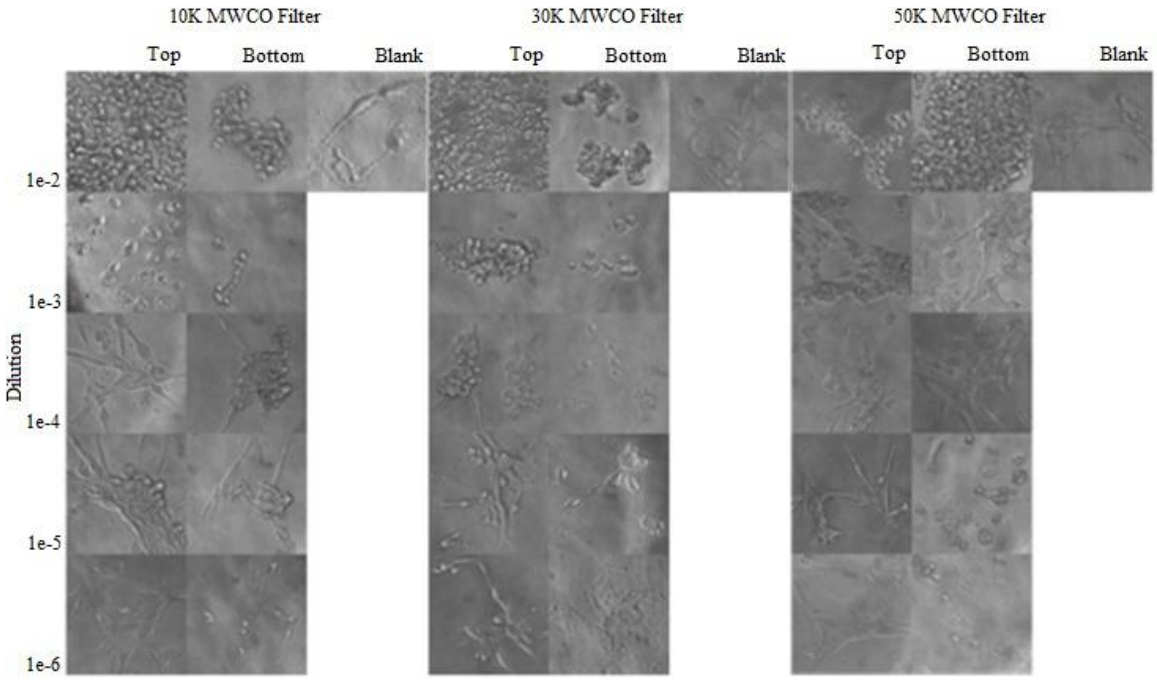

Figure 11: Cells Exposed to 10K, 30K, or 50K MWCO Filtered Venom at Varied Concentration

Figure 11 shows the effect of filtered venom in serial dilution on normal fibroblasts afterfour hours. This was performed in order to determine an appropriate dose at which the cells showed minimal effect. The macroscopic effects are not identical between dosages, but the overall trend was similar: from high to low exposure, cells detached, rounded, and tended to float in large, clumped groups, then floated separately, eventually remaining adherent to the surface of the plate but retaining their rounding. The lowest doses did not affect the extended fibrous arms of the cells and eventually allowed for cells to remain grouped on the plate. The lowest exposure, 1e-6 the original venom concentration, was selected as the safest dosage range observed; a minimal or no effect was recorded at this level.

After four hours of venom exposure, fibroblasts, stained for their nuclei and collagen output, were photographed at 20x; Figures 12 through 15 contain these overlaid images:

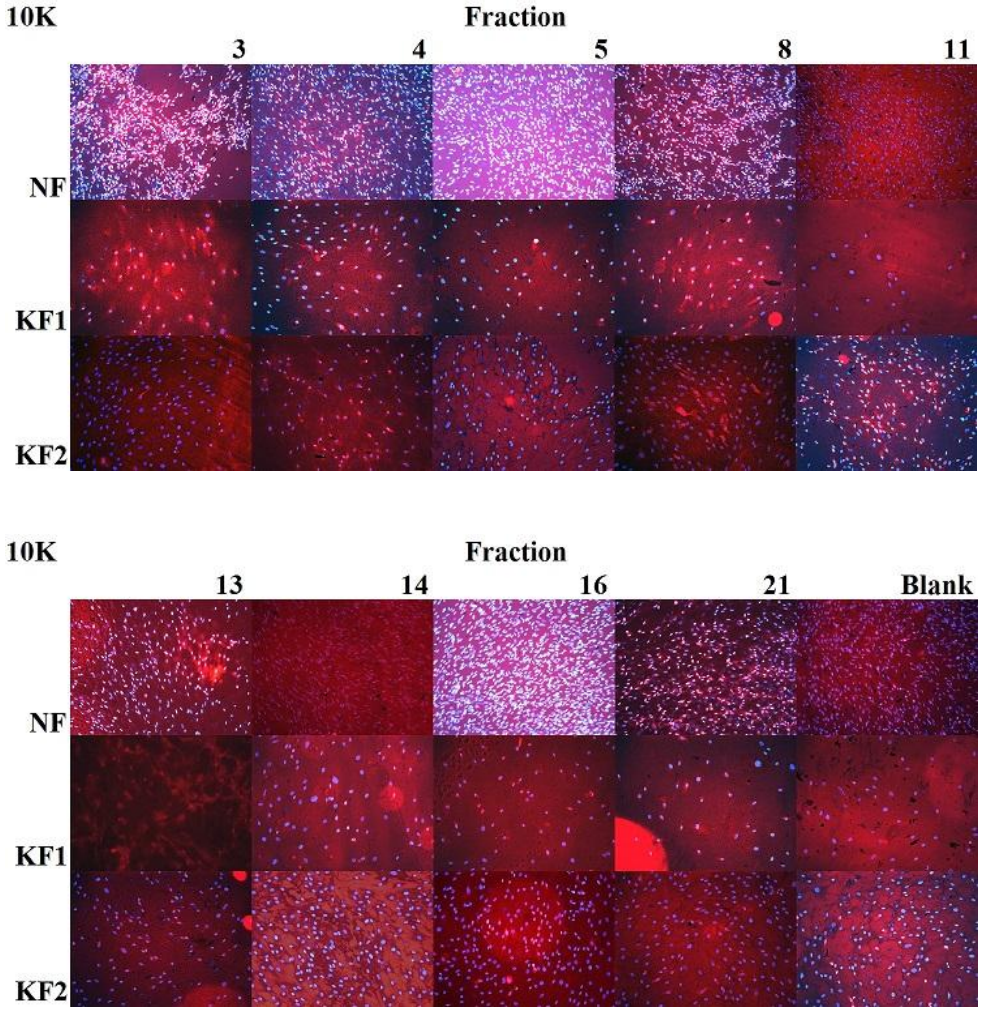

Figure 12: Pictures of Cells Exposed to Venom Fractions from 10K MWCO Filter and Stained for Collagen and Nuclear Information

Compared to controls, some cell lines showed stronger responses over others. For 10K filtered venom, Figure 12, normal fibroblasts clumped with fractions 3 and 8 and cell density rose after exposure to fractions 5, 8, and 16. KF1 cells' nuclei shrank after exposure to fraction 3. Density rose after the addition of fraction 4 and slightly with

fraction 14. Fraction 11 caused density to fall. KF2 density was lower after exposure to fraction 13.

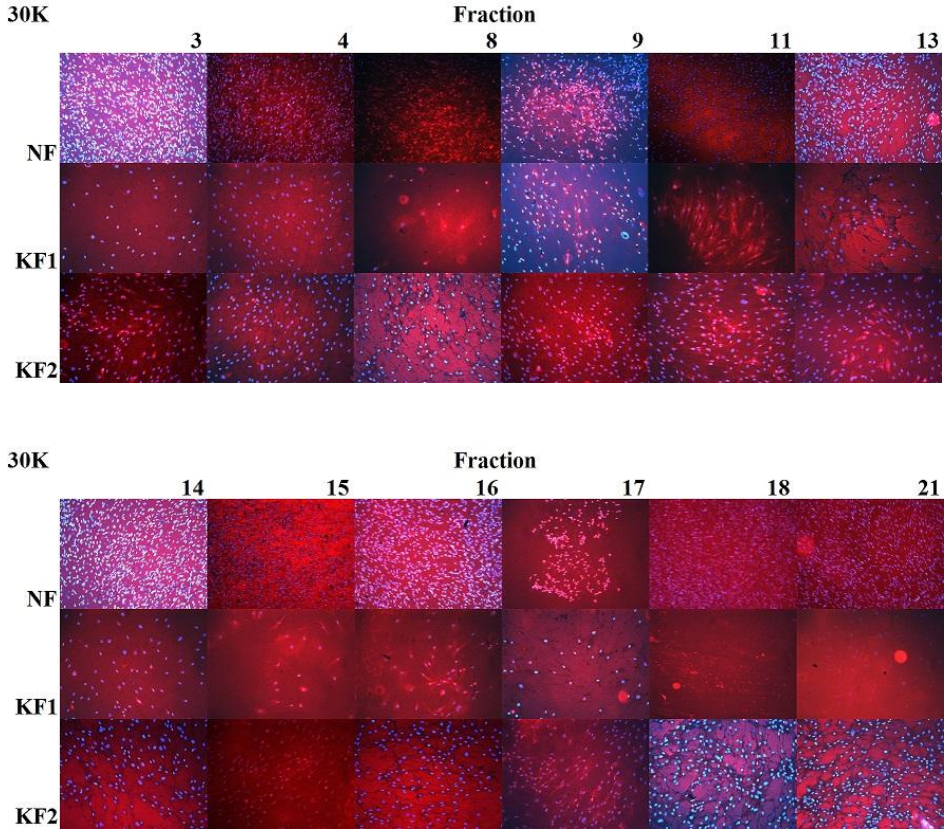

Figure 13: Pictures of Cells Exposed to Venom Fractions from 30K MWCO Filter and Stained for Collagen and Nuclear Information

Fractions from the 30K filter exhibited effects primarily on normal and young keloid cells (Figure 13). Fractions 3, 14, 15, and 16 increased density of normal fibroblasts, while fraction 17 induced clumping. Fractions 8 and 15 lowered seed density and fraction 18 removed all visible cells from the culture. Fraction 13 increased cell density. No significant effects were observed on the late-generation keloid line.

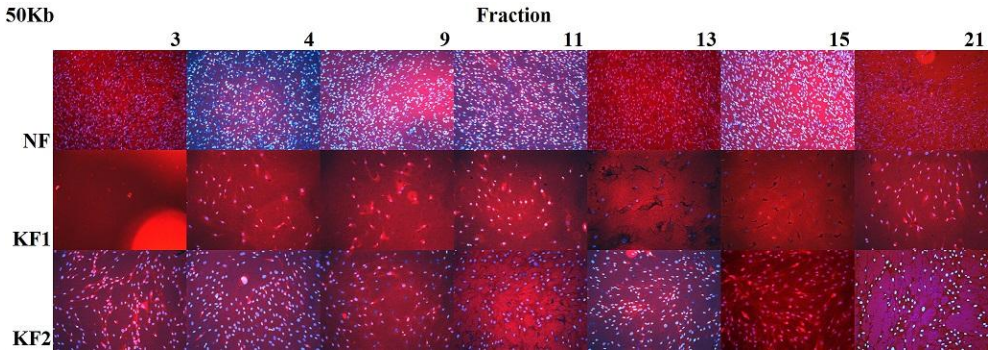

Figure 14: Pictures of Cells Exposed to Venom Fractions from 50Kb MWCO Filter and Stained for Collagen and Nuclear Information

Few effects were noted from the fractions that resulted from the bottoms of the 50K filter (Figure 14). KF1 cells were absent from culture after exposure to fraction 3 and fractions 4 and 9 resulted in lower cell density.

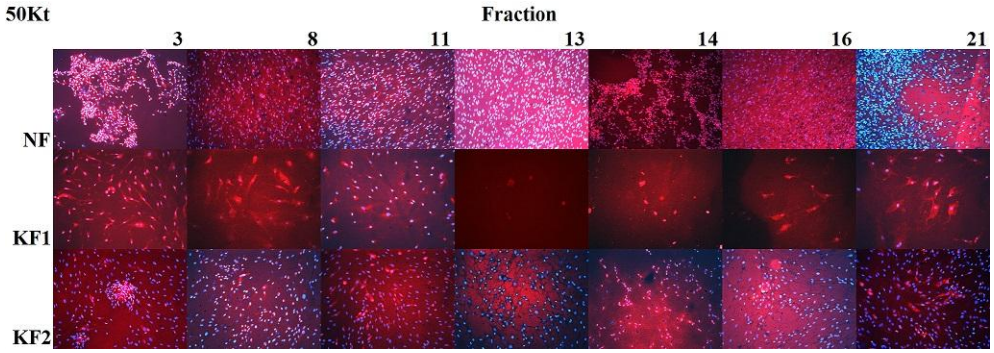

Figure 15: Pictures of Cells Exposed to Venom Fractions from 50Kt MWCO Filter and Stained for Collagen and Nuclear Information

The 50K filter fractions had effects on all cell types (Figure 15). Clumping was observed in fractions 3, 14, and 21 in the normal fibroblast line. KF1 cell density was lowered by fractions 8, 16, and 21, while only acellular debris could be detected after exposure to fractions 13 and 14. Fraction 3 resulted in clumping and fraction 14 caused shrinking of KF2 cells.

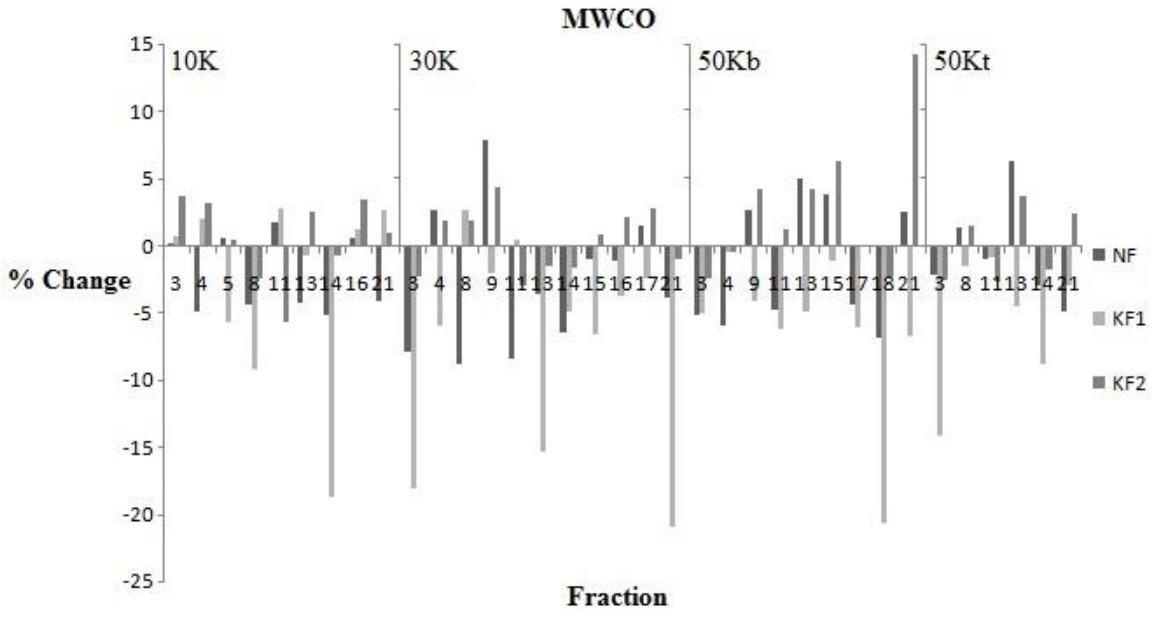

Figure 16: Cell Staining with Propidium Iodide after Four Hours Exposure to Snake Venom

Cells exposed to dilute snake venom fractions for four hours showed a multitude of responses in terms of propidium iodide absorbance as a marker of proliferation; these reactions in terms of percent change are plotted in Figure 16. Dye absorbance was normalized to a control for each cell line. No fractions were observed to negatively affect both keloid lines while simultaneously preserving the normal fibroblast line. Considerable proliferative effects were observed in the young keloid line (KF1) for many fractions. Eleven venom components appeared to inhibit the early-stage keloids while allowing other lines to thrive. These fractions—4 from 10K, 4, 9, and 16 from 30K, 4, 11, and 13 from the 50K bottom, and 3, 11, and 14 from the 50K top—were selected for collagenase activity profiling.

Determine the efficacy of separated venom components at reducing keloid fibroblast phenotypic characteristics such as collagen production

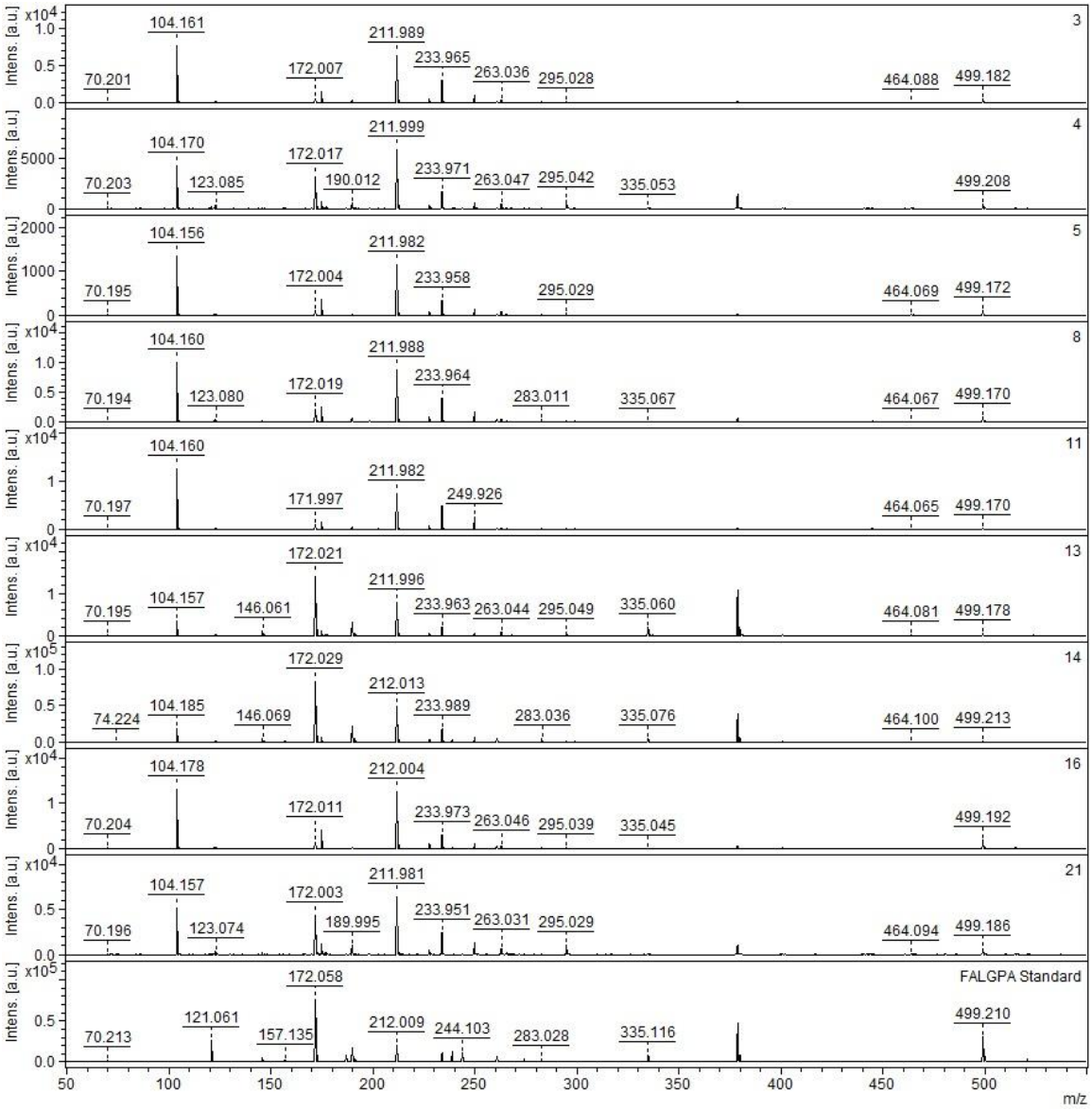

Figure 17: MS of FALGPA Digests of 10K Filter Venom

FALGPA, a known collagenase substrate, was chosen for these experiments due to its commonplace use in determining collagenase activity in unknown enzyme mixtures. The theoretical molar mass of pure FALGPA is 476.53Da. When FALGPA with buffer was assayed on the mass spectrometer directly, this peak was entirely absent. A mass at ~500Da resolved at high intensity compared to all others in the sample; this was

considered to be the substrate and may represent the monosodium salt. A representative spectrum is in Figure 17. Figure 17 displays the digest spectra from the 10K MWCO filtered venom and Figures 36, 37, and 38 (Appendix 1) contains the FALGPA digest spectra from the 30K, 50Kb, and 50Kt filtered venoms. The standard's mass intensity at 500Da was not found to change after samples were subjected to incubation under assay conditions. A drastic change in the mass intensity at this peak was used as a reference for collagenase activity. Although mass spectrometry is a semi-quantitative technique at best, a sharp change in peak height—on the order of ten-thousands of AU—provides a reliable, strict boolean as to whether the peptide was cleaved. The substrate was regarded as degraded by all fractions. Attempts were made to couple the loss of the peak at ~500Da to a gain in some smaller peptide. A mass appeared around 104Da in all fractions which was not present in the control. The only amino acids with masses around this value, with regard to the potential addition of sodium ion, are cysteine and threonine, which are not present in FALGPA. Literature states that bacterial collagenase breaks the substrate solely between the leucine and glycine residues, resulting in hydrolysis product masses of ~244Da and ~250Da. These masses or the addition of these to small group I cations were not observed by the SNAP algorithm. However, given the nonspecific nature of known snake venom enzymes, it is possible that substrate hydrolysis did not cease in the same fashion as bacterial collagenase.

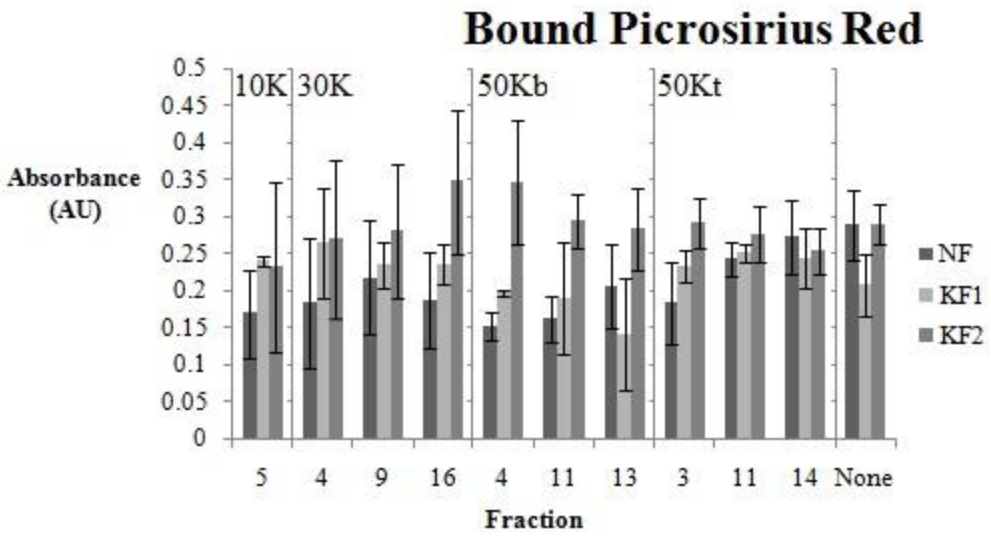

Figure 18: Quantitative Collagen Integrity after 4 Hours Venom Exposure

Fractions which exhibited a negative change over KF1 but a positive effect over the other cell lines were selected from propidium exposure tests to be assayed for their effect on collagen integrity; Figure 18 is plot of the results. The untreated controls possessed similar collagen levels between the normal and second keloid fibroblast lines. The amount of bound Sirius red dye bound by the cell lysates was the least in the NF line and most in KF2 for all fractions except for 13 from 50Kb and 14 from 50Kt. All snake venom fractions reduced the integrity of collagens in fraction normal fibroblasts. The amount of bound dye increased notably in fraction 16 from the 30K filter bottom and fraction 4 from the 50K filter bottom.

Identify proteins and peptides from fractionated snake venom

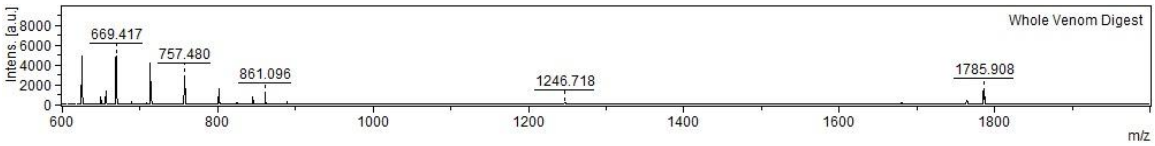

Figure 19: Mass Spectrum of Trypsin-Digested Whole Venom

Figure 19 shows the mass spectrum of whole RDB venom after trypsin treatment. Few major peaks resolved from the digest. No significant peaks resolved above the range displayed. According to theoretical digests of RDB proteins based on literature sources, whole venom contains more resolute peaks than those recorded from our whole venom. Mascot database identified the venom as containing the protein putative secreted protein (Q6MYF5_ASPFU; Aspergillus fumigates, Sartorya fumigate) with a significance score of 60 based on the peptides, while the Uniprot databank searched under the same conditionsidentified the venom as containing the protein polyferridoxin protein vhuB (VHUB_METVO; Methanococcusvoltae) with a significance score of 54. A score of 78 is considered a statistically significant hit in MSDB while a score of 67 is significant in Uniprot.

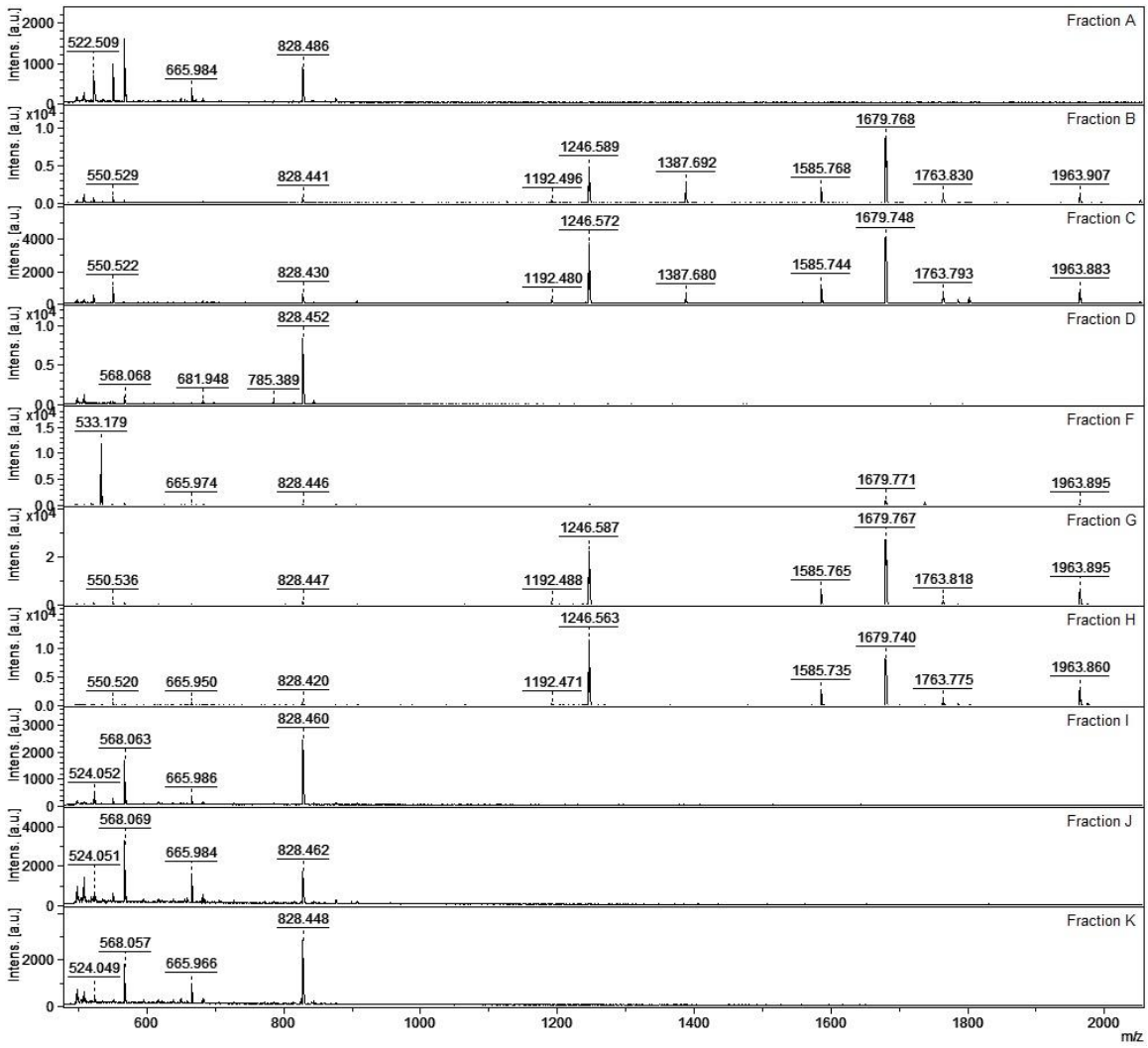

Figure 20: Mass Spectra of Venom Fractions

Figure 20 displays the mass spectra of the fractions after trypsin digestion. Fractions A, I, J, and K were similar as were B and C, and G and H in terms of resolved masses; see Appendix 3 for specific values. Fractions D and F appeared to contain relatively abundant, singular digested peptides, at 828.452 and 533.179Da, respectively. The latter did not appear at appreciable intensity in any other fraction.

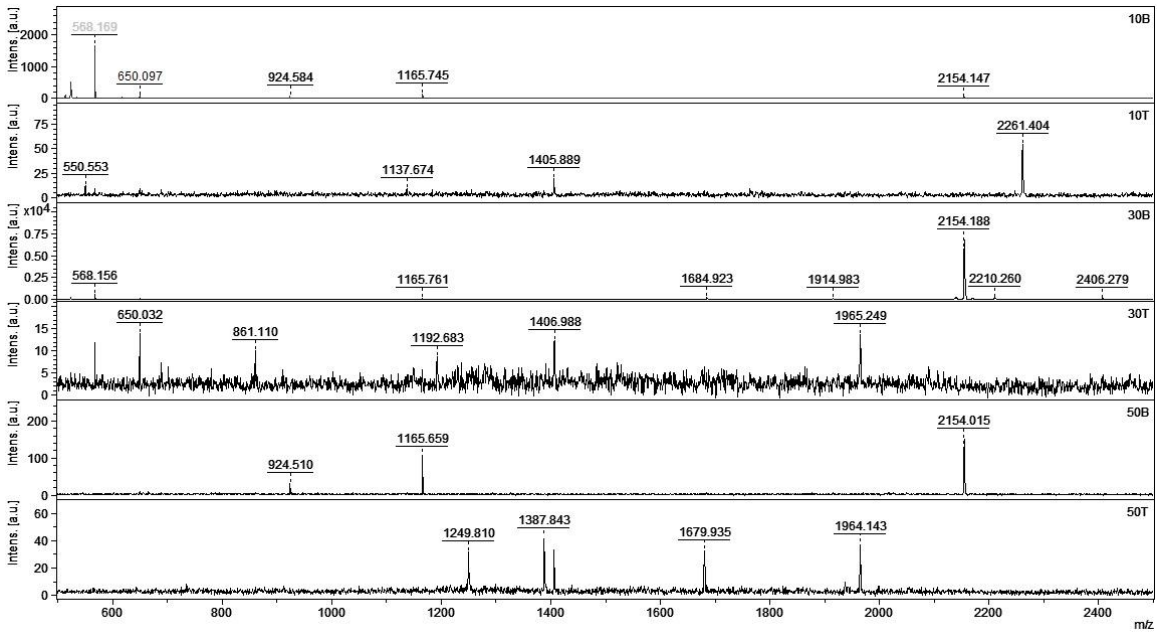

Figure 21: Mass Spectra of Ultrafiltered Venom

Figure 21 shows distinct profiles of post-trypsin-cleaved proteins resulting from the ultrafiltration of RDB venom. The same derived masses that passed through the filters, such as 1165 and 2154, and the retained mass of 1405, were consistent among all three runs, while each fraction possessed unique peaks that were not observed in the other runs, such as 2251 in the top (retentate) of the 10K filter, 2405 in the bottom (permeate) of the 30K filter, and 1249 in the top (retentate) of the 50K filter.

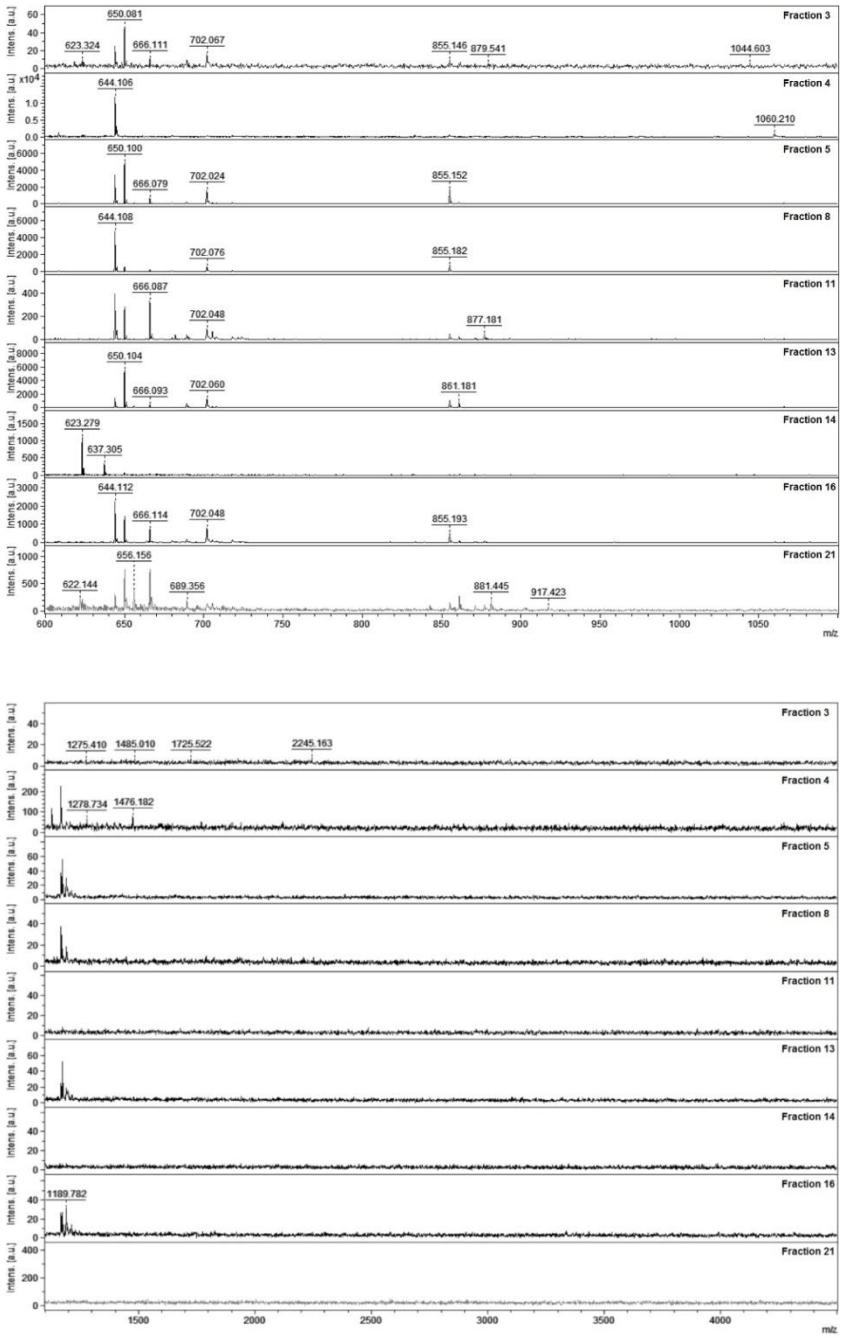

Figure 22: Mass Spectra of FPLC-Processed Fractions from 10K Filter from 600-1100Da and 1100-4500Da

Figure 22 shows the mass spectra of venom after ultrafiltration through a 10K filter, FPLC processing, trypsinization, and ziptipping. All fractions contain fragments of 644

or 650 and 855 or 861Da with the exception of fragments 7, which contains neither, and 2 and 5, which do not contain the high-MW peptides. A mass around 523Da was observed in fractions 1, 7, and 10. Fractions 5, 7, 9, 10, and 11 gave little contrast in the mass spectrometer above 1100Da. A mass around 1189Da was measured in fractions 2, 3, 4, 6, and 8. Fractions 1 and 2, the injection peaks, contained mass intensities around 1276 and 1485.

Figures 25 and 26 (Appendix 1) show the mass spectra of venom after ultrafiltration through a 30K filter, FPLC processing, trypsinization, and ziptipping. Barring the fifth fraction, all separations possessed intense masses around 644 or 650, 702, and 855 or 861. Fraction 4 has a 1046Da peak in noticeable quantity, and fractions 2, 5, and 7 have a 623 peak varied within the range of a small number of electron masses. Many of the spectra are flat above 1100Da, though an 1189 peak was observed in fraction 1. Unique masses were recorded in fractions 2, 4, 5, 8, 10, and 11, but most lacked stark contrast overall.

Figure 27 and 28 (Appendix 1) show the mass spectra of venom after ultrafiltration through a 50K filter, FPLC processing, trypsinization, and ziptipping. All fractions selected in this range possess peaks around 644 and 855 or 861 and, except for the sixth, one at 702. Fraction six shares a peak around 689 with fraction five and has a unique peak at 893.

Figure 29 and 30 (Appendix 1) show the mass spectra of venom that was retained in the top of a 50K filter after ultrafiltration, FPLC processing, trypsinization, and ziptipping. The spectrum for the first fraction was nearly empty of real data under 1100Da, but the

rest contained masses at 644 or 650, 689 or 702, and 855 or 861. Fraction 3 had a peak around 1189, fractions 1, 4, 5, and 7 had a peptide around 1246, and fractions 1, 2, 4, and 5 each had one around 1679. The rest of the samples provided weakly-contrasted spectra.

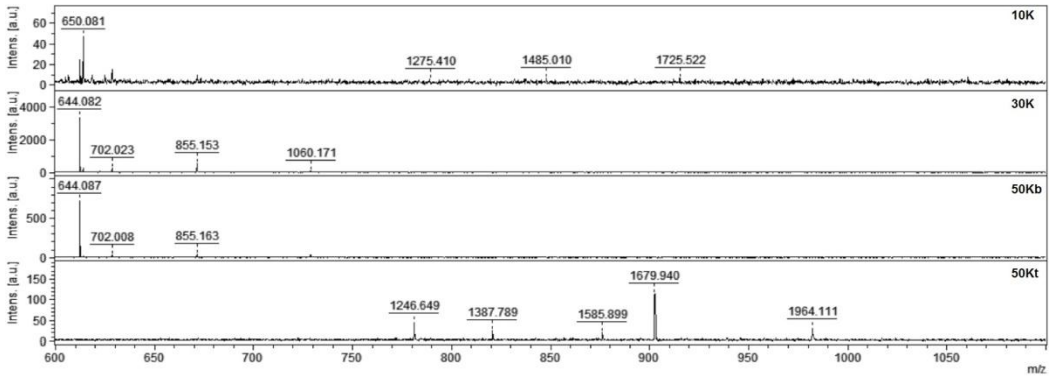

Figure 23: Comparison of Fraction 3 (Injection Peak) from Venom Filtrations

Notably different masses resolved between the various fraction volumes from the FPLC, considering that the conditions at which the machine was ran were the same per trial. The peptides resolved separately in the 3rd, 11th, 14th, and 21st fractions (Figure 23 and Figures 31, 32, 33, 34, and 35; Appendix 1) were quite distinct; those in the others were similarly distributed. The 30K and 50Kb cutoffs filtered like mass profiles in the injection effluent, e.g. fraction 3. Nearly all fractions, no matter the filter, contained a peak around 644 or 650Da.

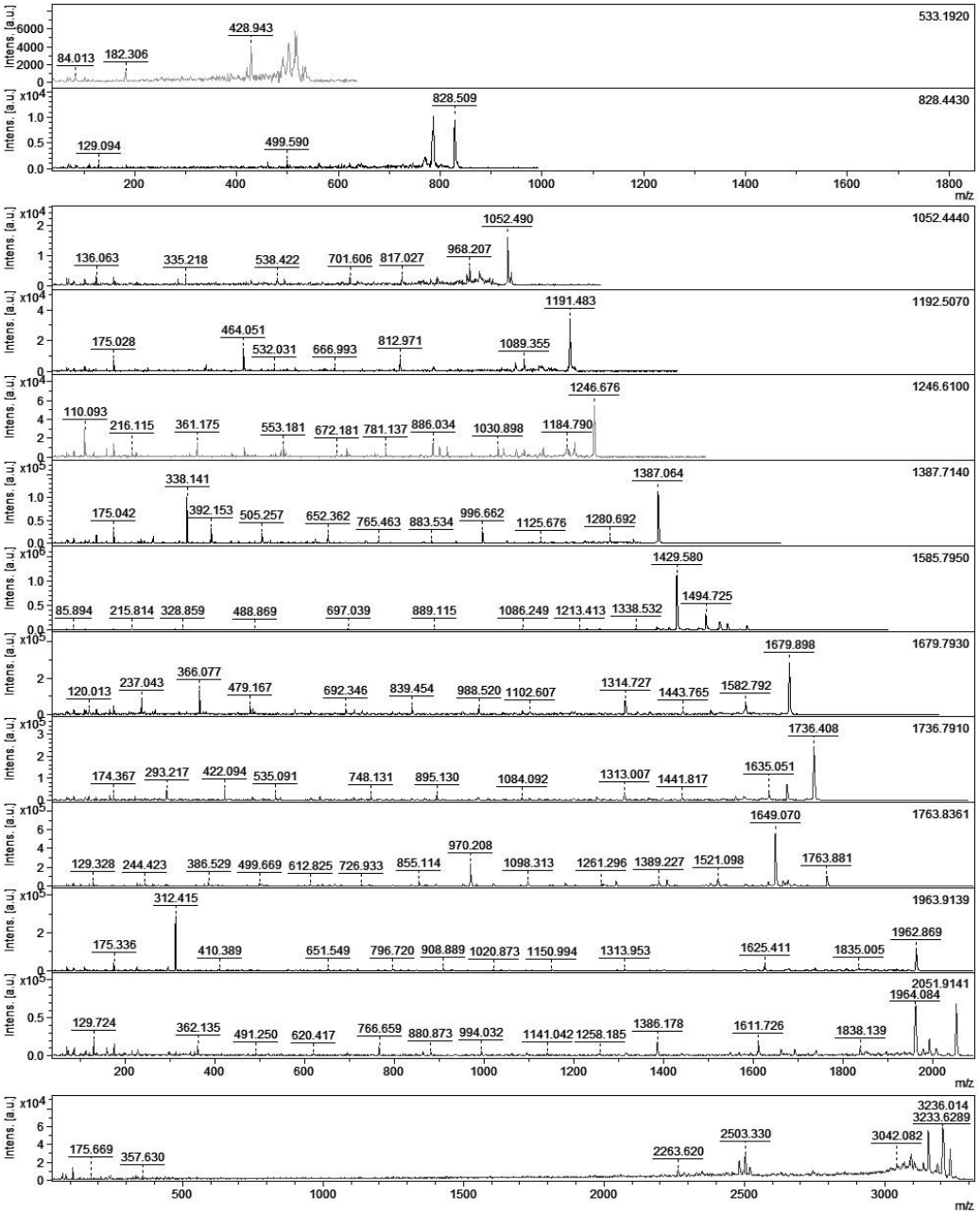

Figure 24: Representative Mass Spectra of LIFTs Performed on Venom Fractions

Figures 24 and Figure 39(a-c) (Appendix 1) displays the LIFTs performed on prominent peaks found in refined, digested *C.r.r.* venom. The distances between the initial peaks in the 855, 861, and 877Da LIFTs were similar, as were those between 1060 and 1066, and 4198 and 4312. Intermediate masses generated during LIFT that were present in multiple

fractions within a 1Da tolerance included 175 in 1933, 1943, 1964, 2186, and 2316, 704 in 889 and 893, 750 in 4198 and 4312, 871 in 1060 and 1249, 889 in 1585, 2709, and 3315, 1758 in 1933 and 1943, and 3485 in 4198 and 4312. Intermediate peaks which were identified by the default Bruker LIFT method that matched parent masses within a 1Da tolerance included 855 in 1047, 861 in 889, 877 in 1066, 889 in 1585, 893 in 1268, 1060 in 1249, 1287 in 2709, and 2187 in 2316. LIFTs performed below 855Da produced irresolute spectra with neither peaks nor any chosen by the SNAP algorithm and are not displayed here.

Table 5: Proteins Identified in Fractions Indicated via MALDI-TOF with Statistical Significance

MWCO	Fraction	Database	Protein	Peptides	Obs.	m_r(expt)	m_r(calc)	Significance	Criteria (>)
50Kt	3	MSDB	Ruberlysin (EC 3.4.24.48)	K.NTLHSFGEWR.K	1246.6490	1245.6417	1245.5891	71	44
50Kt	3	Uniprot	Ruberlysin (EC 3.4.24.48)	K.NTLHSFGEWR.K	1246.6490	1245.6417	1245.5891	71	36
50Kt	8	MSDB	Ruberlysin (EC 3.4.24.48)	R.VHEIVNFINEFYR.S	1680.1081	1679.1009	1679.8467	104	44
50Kt	8	Uniprot	Ruberlysin (EC 3.4.24.48)	R.VHEIVNFINEFYR.S	1680.1081	1679.1009	1678.8467	104	35
50Kt	13	MSDS	Ruberlysin (EC 3.4.24.48)	K.NTLHSFGEWR.K	1246.6890	1245.6818	1245.5891	71	44
50Kt	13	Uniprot	Ruberlysin (EC 3.4.24.48)	K.NTLHSFGEWR.K	1246.6890	1245.6818	1245.5891	71	35
50Kt	14	MSDB	Ruberlysin (EC 3.4.24.48)					208	44
				R.SYEFSDASMR.Y	1192.5869	1191.5796	1191.4866	33	
				K.NTLHSFGEWR.K	1246.7009	1245.6937	1245.5891	71	
				R.VHEIVNFINEFYR.S	1679.9978	1678.9906	1678.8467	104	
50Kt	14	Uniprot	Ruberlysin (EC 3.4.24.48)					208	35
				R.SYEFSDASMR.Y	1192.5869	1191.5796	1191.4866	33	
				K.NTLHSFGEWR.K	1246.7009	1245.6937	1245.5891	71	
				R.VHEIVNFINEFYR.S	1679.9978	1678.9906	1678.8467	104	

Few coupled MALDI-TOF and LIFT datasets provided statistically-significant evidence that the venom fractions contained previously-characterized and sequenced proteins in MSDB and the Swissprot database. Table 5 contains the significant data and Table 6 (Appendix 2) contains data from earlier database searching that used a broad mass tolerance of 800ppm. The only fractions to contain these proteins were in the top of the 50K filter and all of them were identified as ruberlysin. Because ruberlysin's mass is ~24kDa, it is possible that there is either at least one similar metalloprotease in the venom with a high molecular weight such as the one previously named "HT-3" or that ruberlysin's size restricts it from passing through the 30K and 50K filters efficiently. Both the injection fraction (fraction 3) and others that passed through the FPLC indicated ruberlysin as well, implying that the protein quantity is high enough to contaminate more samples than the restrictions set by the physical limitations of the buffer system can overcome. Many other fractions from all filtrations possessed masses that matched or were similar to those described in theoretical digests of the RDB proteins found in

databases. Some of these masses include 1192Da, 1246Da, and 1679Da. Theoretical digests are provided in Appendix 4.

IV. DISCUSSION

Develop a working scheme to isolate single proteins and peptides from red diamondback venom

The combination of ultrafiltration and FPLC results in a cost- and time-effective partitioning system for snake venom proteins and peptides. Sample mixtures can be reliably resolved into components within hours, depending on the rate of buffer dialysis after FPLC treatment.

After one passage through our FPLC, mild separation of proteins and peptides was attained. The mass spectra of the ten fractions showed two basic fragment profiles and all of them returned similar results after database searching [Newman, 2012]. Simple ultrafiltration of snake venom showed consistent separation of proteins and peptides: the same fragments were observed after trypsinization after passage through filters, e.g. a fragment around 1405Da resolved in the bottom of the 30K and 50K filter but not the 10K filter, when sizing membranes were the only mode of separation employed.

When the techniques were used in tandem, this patterning does not appear to be so clear-cut. This may be due to the presence of multiple snake venom metalloproteases of different size classes in red diamondback venom: the active site is heavily conserved and the trypsinized fragment is likely to be similar or the same among most venom metalloproteases, but the complete secreted protein may already be partially cleaved by the venom itself during in vivo processing and secretion or laboratory handling of the product. Lyophilization, the first step in handling venom once it has left the animal,

concentrates the sample into a solid that brings all components into direct contact with one another. Similarly, the usage of buffers during separation provides charged and steric cofactors that may modulate the proteolytic activity implicit in red diamondback venom. The presence of serine proteases and the nonspecific action of SVMPs coupled to their dimer- and trimer-forming sites may allow early destruction of whole proteins. PII, PIII, and PIV SVMPs are described as long-chain metalloproteases with individually-active moieties such as lectins, phospholipase A2s, and disintegrins. A few specific sites on long-chain metalloprotease may be preferentially autolyzed during venom production and this process may result in the sequestration of these moieties as individual proteins. For example, myotoxin (Swissprot accession P24330) shows a high homology when queried against snake metalloproteases (The Uniprot Consortium, 2013). However, the individual moieties present in the metalloproteases in *C.r.r.* venom may not necessarily fall prey to this type of cleavage; instead, structural damage may result to the quaternary structure of the intact protein.

Evaluate the ability of separated *C.r.r.* venom to cause proliferation or death on keloid scar and normal dermal fibroblasts.

Many effects were observed after the application of *C.r.r.* venom to dermal fibroblasts. MTT assay provided evidence of cell inhibition in all fractions and time-response photography showed signs of inhibition or loss of cells in all fractions. Some of the effects were immediate and others were gradual; this may be purely to the quantity of venom in each fraction. One technique used in literature to determine concentration is based on the absorbance output from FPLC separations, but this measurement requires at least one venom fraction to have a known protein concentration, and Bradford's assay did

not reliably detect protein in a single fraction. The same effects of the time-response—initial exposure leading to cell rounding and floating, living cells adhered back to the plate, regenerated their spindles, and spread out across the wells—were observed from a high to low venom dose. Quantitative propidium iodide staining gave mixed results in that no fractions appeared to minimally or positively impact normal fibroblasts while perturbing both keloid lines. The most prominent effects were observed over the young keloid fibroblast line. These effects were reinforced by the results gathered by photography of all three cell lines after staining for nuclear information and collagen: few living cells or only debris was left after exposure to the most fractions. Normal fibroblasts, which exhibited a high endogenous density and replication rate, showed the most positive changes toward proliferation.

Determine the efficacy of separated venom components at reducing keloid fibroblast phenotypic characteristics such as collagen production.

Our intention in testing the capacity of our venom to break down collagen was so that we could verify the absence or presence of metalloproteases in the venom. Although serine proteases may cleave collagen, this activity has not been described in*C.r.r.* venom up to this point and was not considered during study. FALGPA was chosen for initial studies due to its prevalence in the characterization of collagenolytic activity of bacterial collagenases used in research. Few fractions completely degraded the 500Da peak that our studies attributed to FALGPA entirely but all reduced its intensity to near-zero. Because mass spectrometry does not perform accurate quantitative measurement and SVMPs are not exclusively active on peptide substrates, the data derived from this assay

is not a clear-cut indicator of the absence or presence of metalloproteases. However, given our results from literature review, venom component identification, and results from collagen activity assay from whole cells, it is reasonable that all fractions may contain at least some trace but significant amount of metalloprotease.

Identify proteins and peptides from fractionated snake venom.

LIFT analysis of whole venom and its constituents provided a variety of data after query against the Swissprot and MASCOT databases. Numerous vertebrate toxins, including skin-derived non-human antimicrobial peptides, primate defensins, and snake metalloproteases were returned but none of the former and few of the latter came back with statistical significance. A preliminary set of data is provided in Table 6 (Appendix 2) and a finalized chart of statistically significant data is provided in Table 5 (Appendix 1). The only metalloprotease to be clearly defined after LIFT was ruberlysin.

Some of the peaks observed after FPLC separation that were analyzed by LIFT were not clearly defined in the fractions. The parent spectra of these sequences, such as that derived for a peak between 1165 and 1169 in fractions 4, 5, 8, 16 in from the 10K filter, 9 and 13 from the 50K bottom, and 11 from the 50K top were nondescript about the ranges when tested at one-dalton intervals. A peak at 1165 was selected as parent because it produced the cleanest spectrum and may have altered the search algorithm parameters significantly.

The abundance of these fragments among multiple fractions may imply the presence of sequentially different constituent peptides. A standard isotopic distribution is typically observed in a 3-Dalton range for biological material unless it is sulfur-abundant. Due to

red diamondback venom having been described as containing an alternatively-spliced or mutant metalloprotease, which differs from ruberlysin by four amino acids and the numerous other small chain-variant snake venom proteins that have been established in literature, it is possible that the fractions containing unidentifiable parent fragments carry alternative forms of similar sequences. Similarly, the fragmentation spectra of numerous parent ions show a variety of degenerate masses that may show missed cleaves by trypsin or single amino acid substitutions; these are detailed in the "results" section. It is entropically favorable for isosteric or physiochemical homologous masses to aggregate during separation processes so some of these peptides may persist among multiple fractions.

V. CONCLUSION

The red diamondback venom used in our studies contains proteins and peptides that have not been sequenced previously and are not present in the databases used in our search. Peptide fragments at or close to those which are generated after trypsin digest, such as that at 1585Da, that are present in multiple fractions of our venom have not been described in any red diamondback literature to our knowledge. However, our search proved fruitless in sequencing the entirety of one of these novel proteins. Ruberlysin, the only protein to be identified significantly, appeared in the top of the 50K filter, but its mass should have forced it to pass through during 30K and 50K ultrafiltration processes.

The separation techniques employed in this study were limited in grasp but showed a cost- and time-effective means of efficiently separating the contents of complex protein mixtures. Future work on this end of the project may include refining the FPLC buffers and their mixing rates within the system, adding a metalloprotease inhibitor to the venom that does not affect trypsin, such as 1,10-phenanthroline, and further testing the activity of the fractions to verify the presence or absence of metalloprotease. A longer FPLC separation using a taller column may account for these errors outright.

The development of a fast spectrophotometric assay for metalloprotease presence would be useful for future the rapid screening of separated venom. Attempts made using FALGPA for this failed to give results.

The cells used in this study gave valuable results with regard to how different types of dermal fibroblasts react to enzymatic subjugation. The age of the cells, i.e. how long they had been isolated in culture may be a relevant focus for future keloid research with regard to snake venom. Many snake venom fractions, especially those which showed minimal effect on normal fibroblast cells and pronounced effects on the keloids, may be of pertinent interest for therapeutic use; in this vein, longer time-response trials are required to eke out the real potential of the venom. All of the photographs of cells give a direction for the time and dose required of the venom proteins and peptides, but much more quantitative data is necessary for a valid assessment of the venom to be made.

VI. APPENDIX

APPENDIX 1: RESULTS

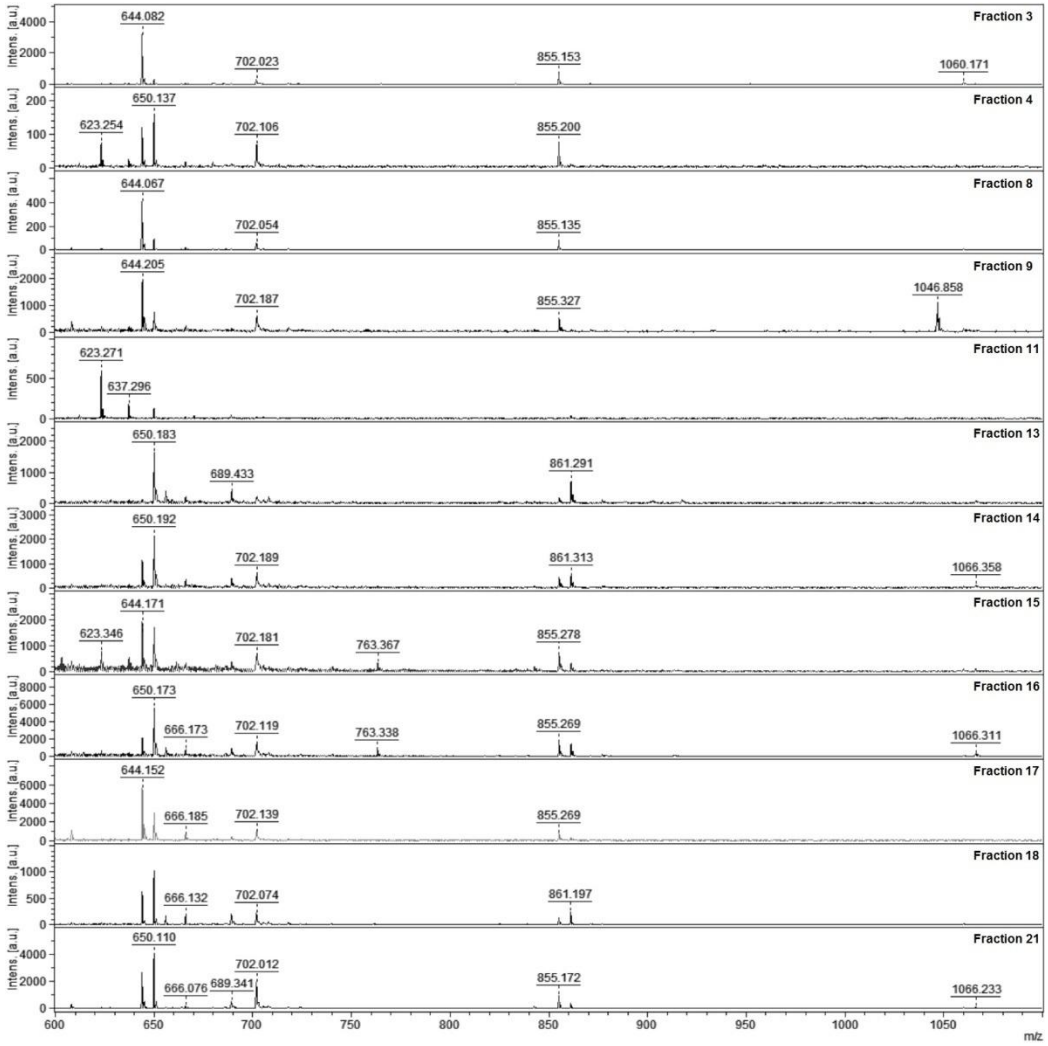

Figure 25: Mass Spectra of FPLC-Processed Fractions from 30K Filter from 600-1100Da

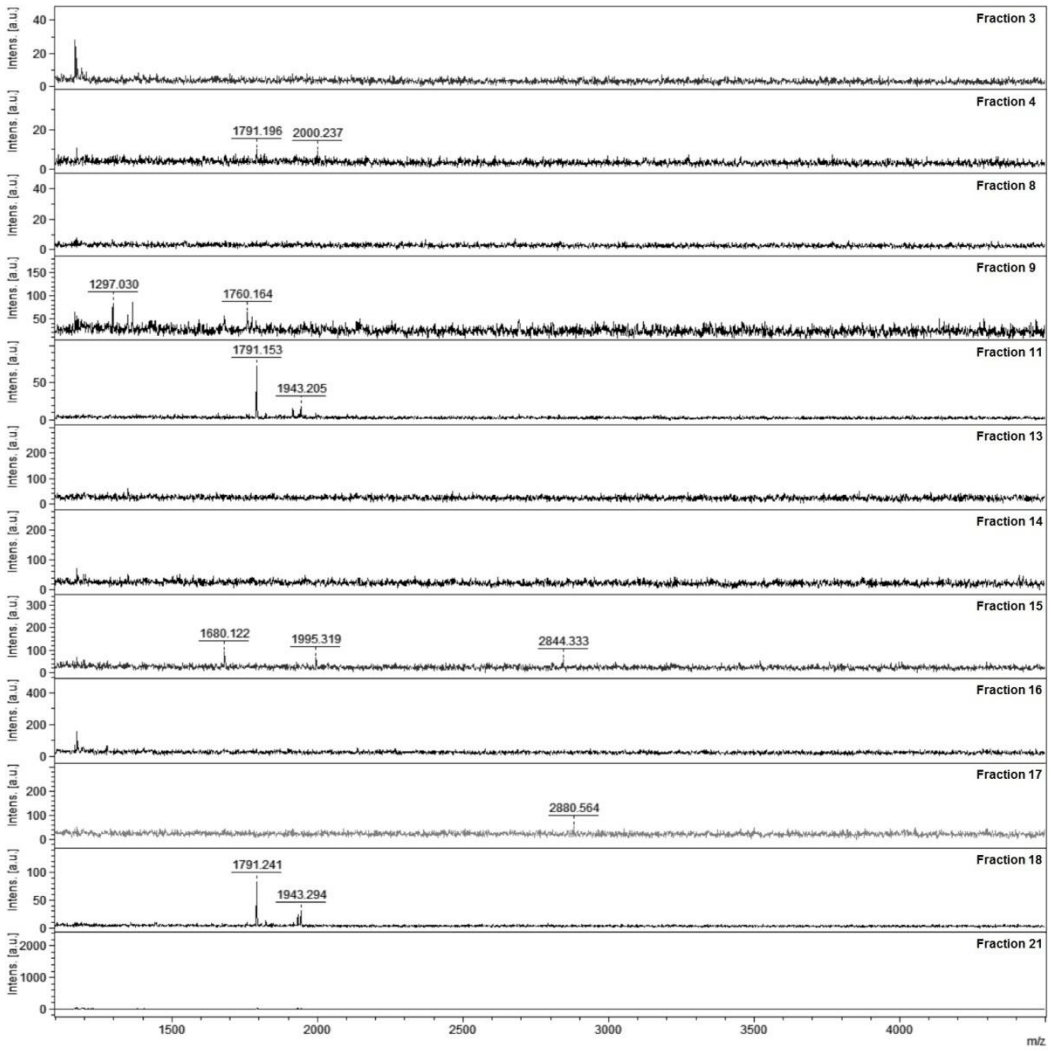

Figure 26: Mass Spectra of FPLC-Processed Fractions from 30K Filter from 1100-4500Da

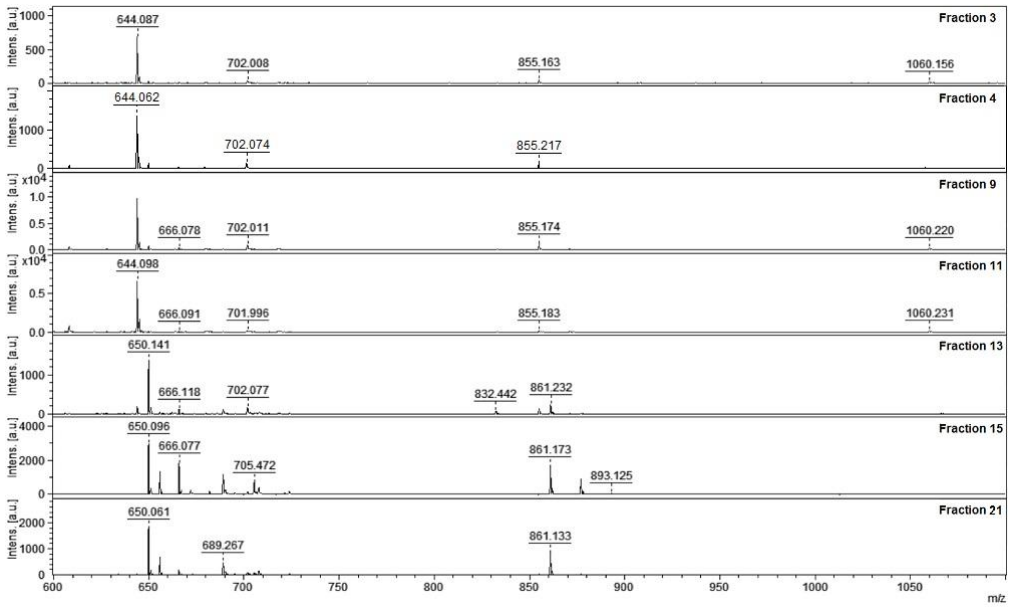

Figure 27: Mass Spectra of FPLC-Processed Fractions from 50Kb Filter from 600-1100Da

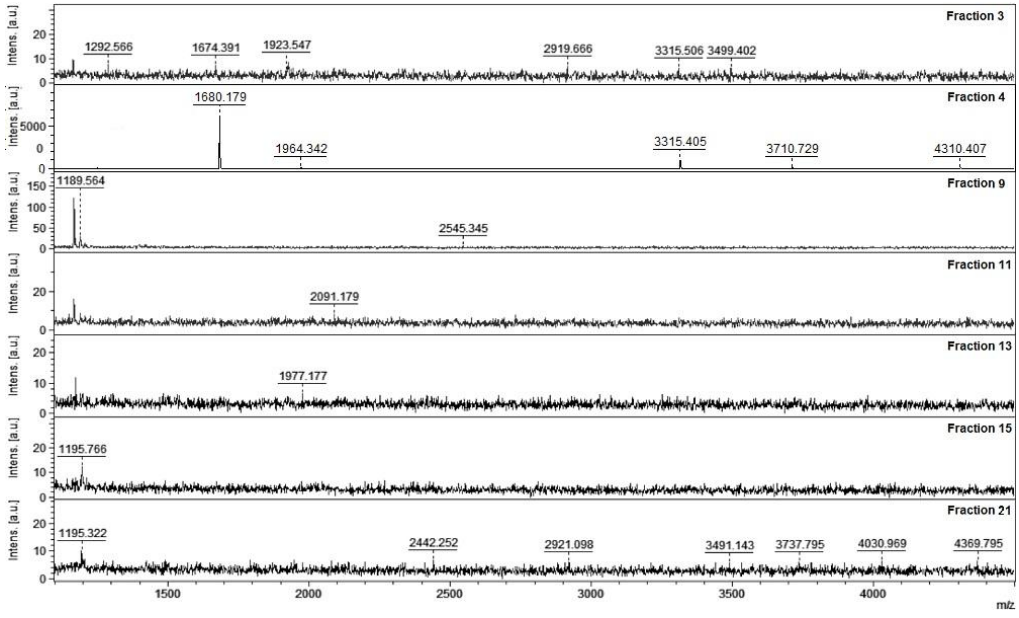

Figure 28: Mass Spectra of FPLC-Processed Fractions from 50Kb Filter from 1100-4500Da

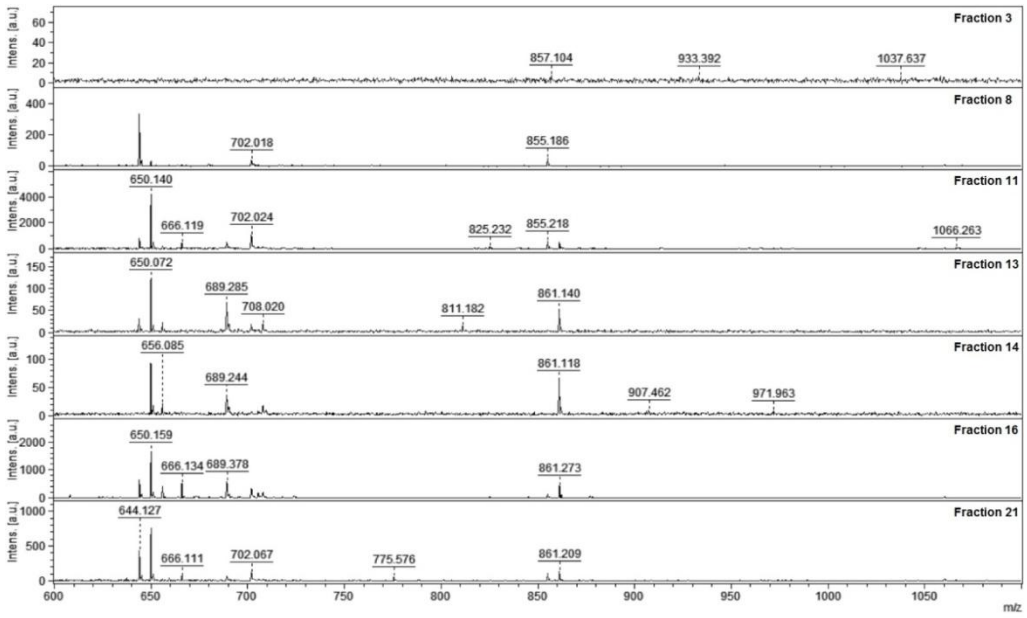

Figure 29: Mass Spectra of FPLC-Processed Fractions from 50Kt Filter from 600-1100Da

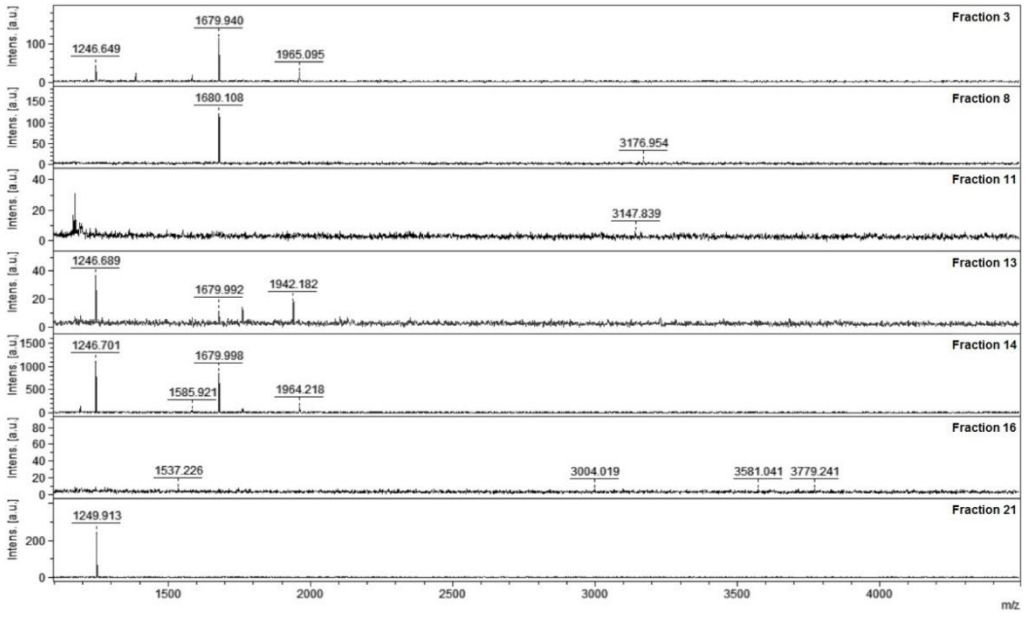

Figure 30: Mass Spectra of FPLC-Processed Fractions from 50Kt Filter from 1100-4500Da

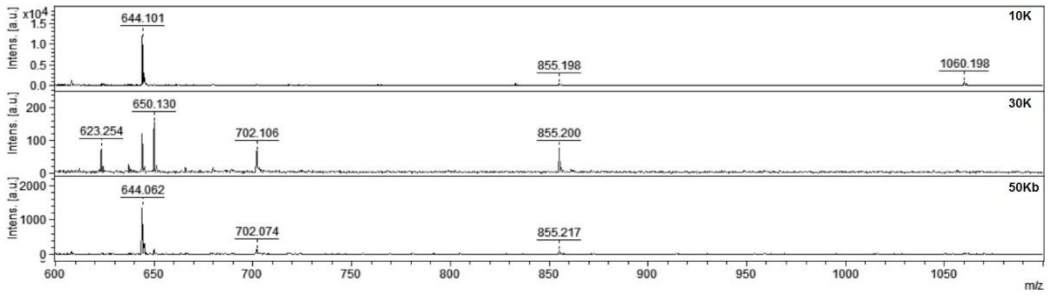

Figure 31: Comparison of Fraction 4 MS from Venom Filtrations

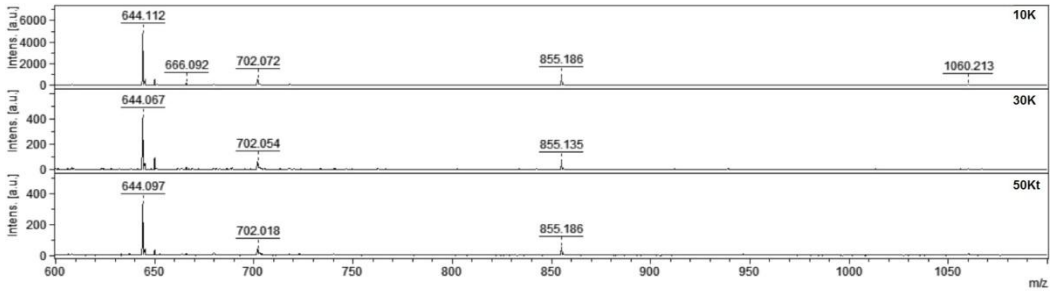

Figure 32: Comparison of Fraction 8 MS from Venom Filtrations

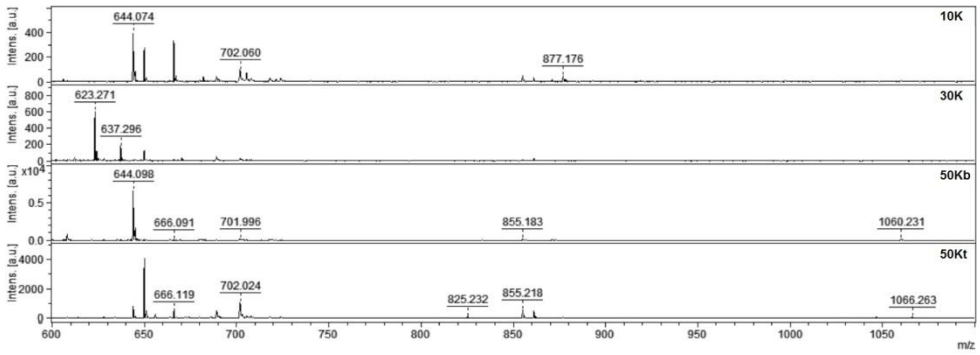

Figure 33: Comparison of Fraction 11 MS from Venom Filtrations

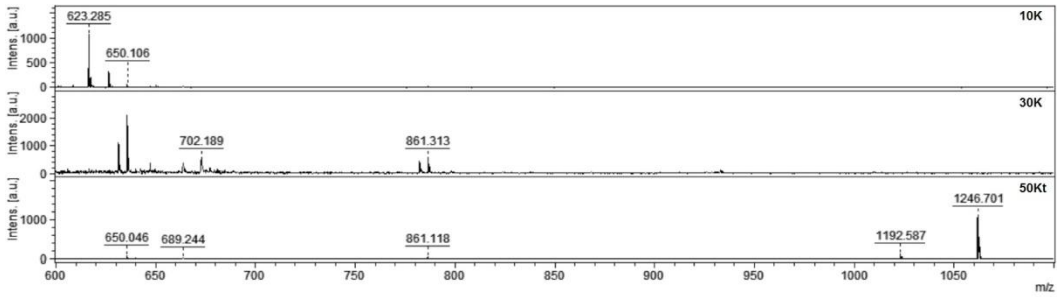

Figure 34: Comparison of Fraction 14 MS from Venom Filtrations

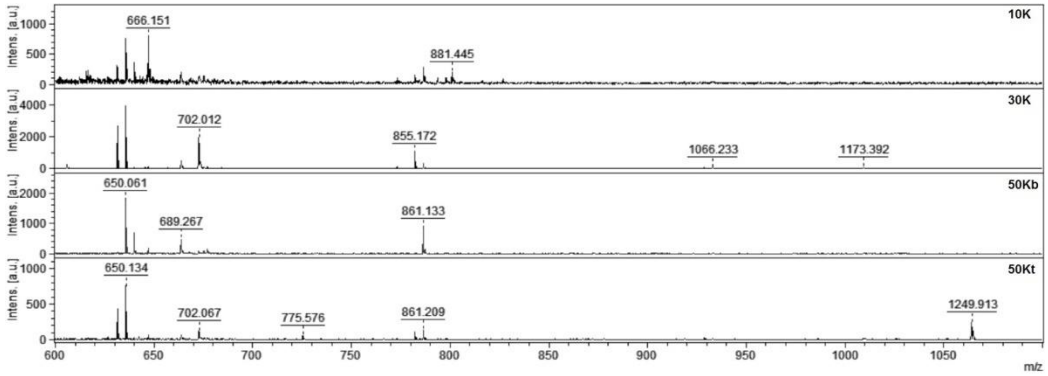

Figure 35: Comparison of Fraction 21 MS from Venom Filtrations

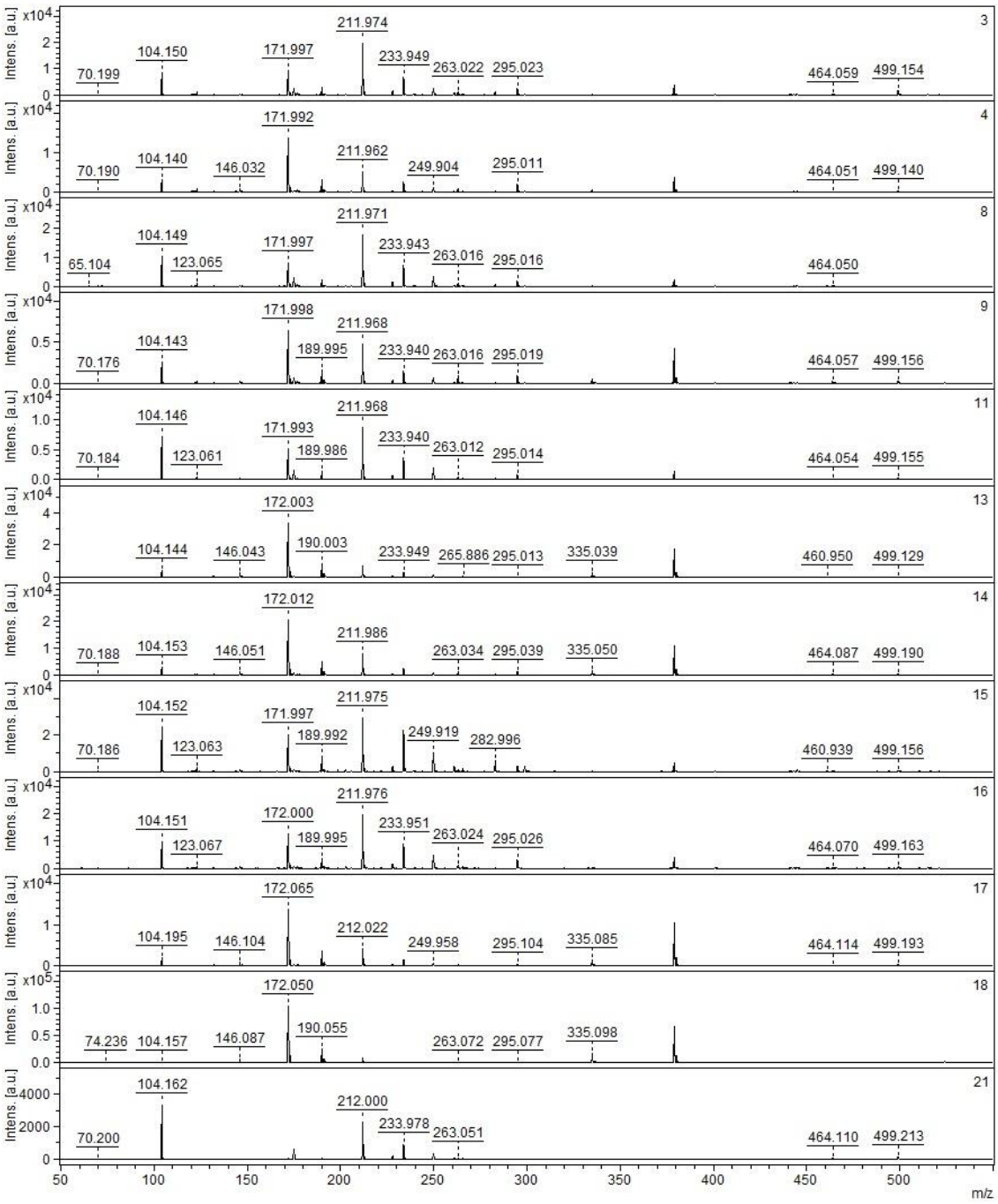

Figure 36: MS of FALGPA Digests of 30K Filter Venom

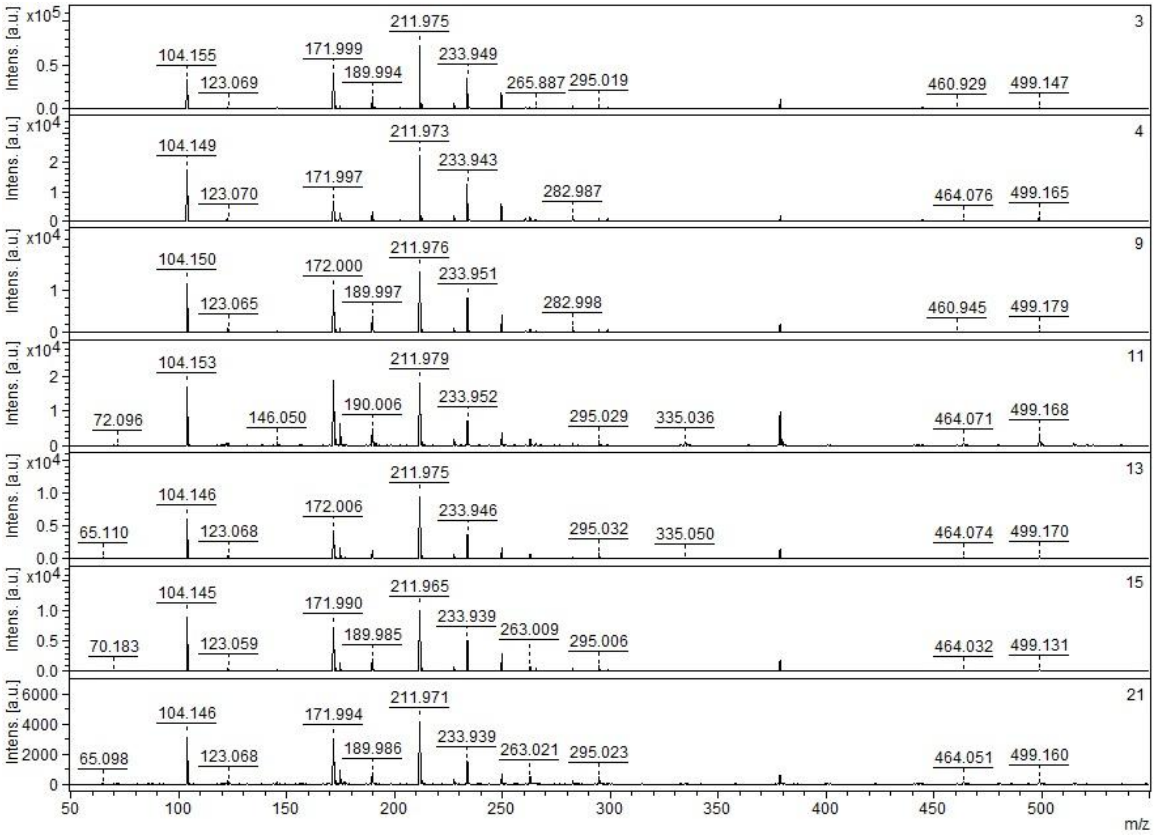

Figure 37: MS of FALGPA Digests of 50Kb Filter Venom

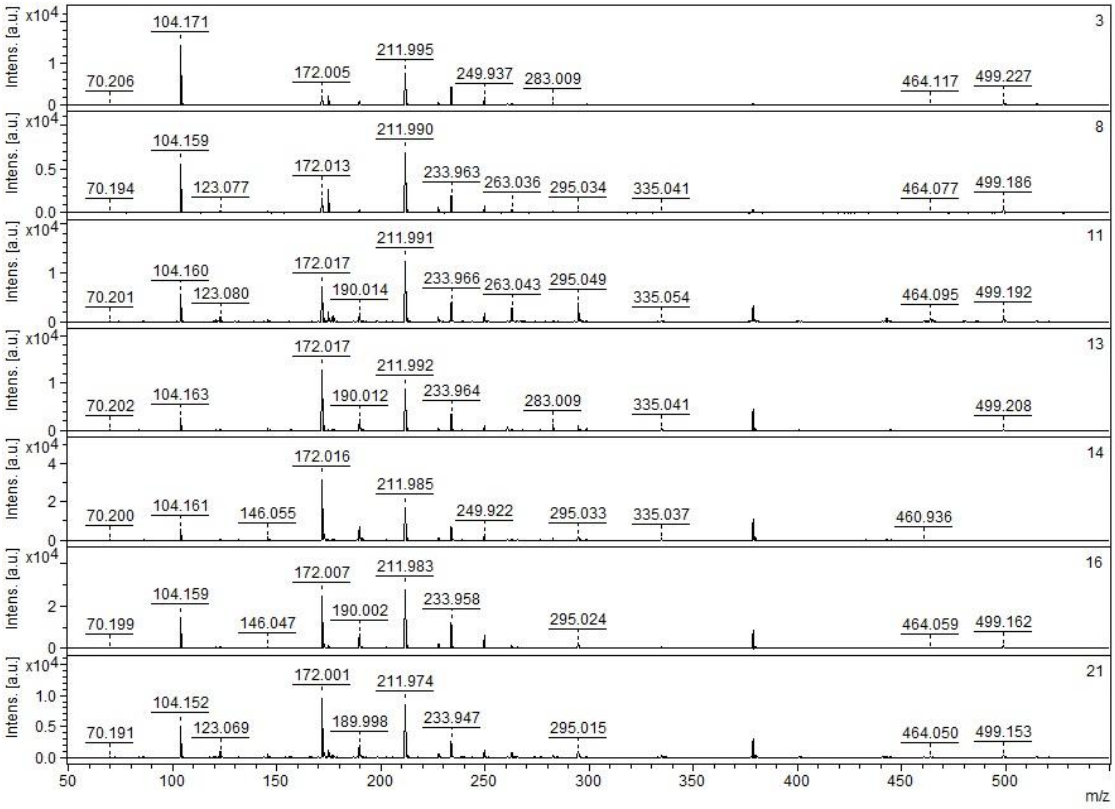

Figure 38: MS of FALGPA Digests of 50Kt Filter Venom

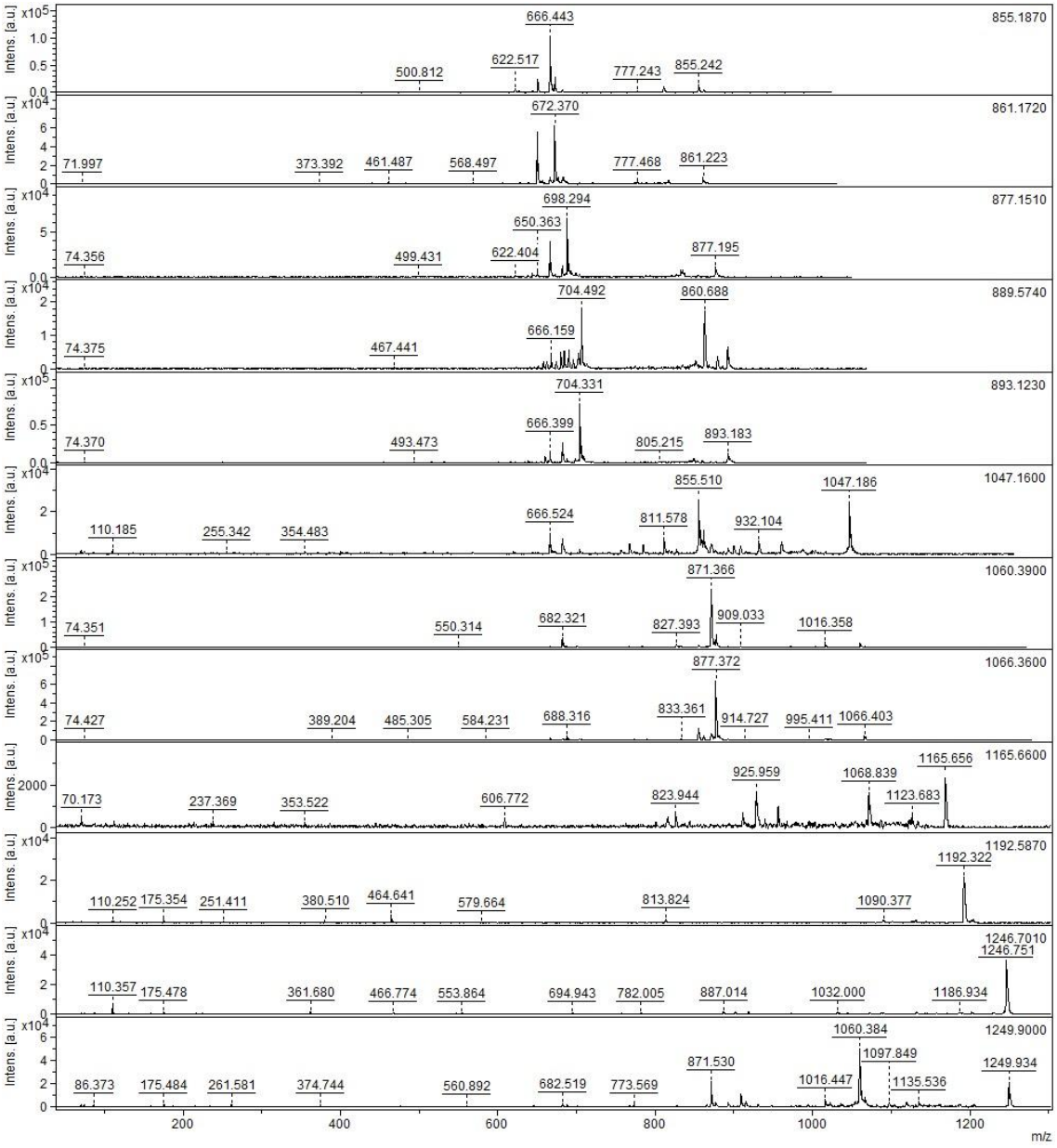

Figure 39a: Mass Spectra of LIFTs Performed on Venom Fractions

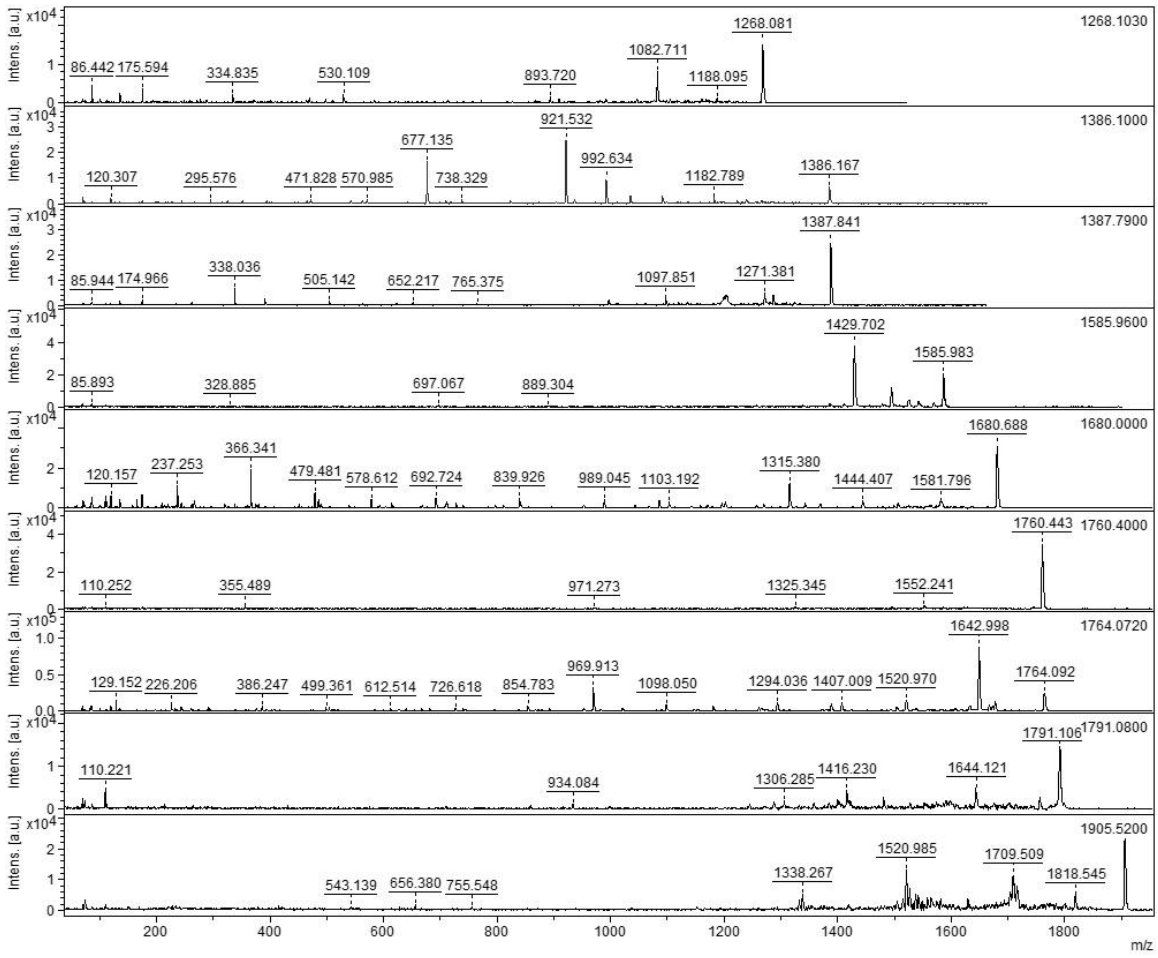

Figure 39b: Mass Spectra of LIFTs Performed on Venom Fractions

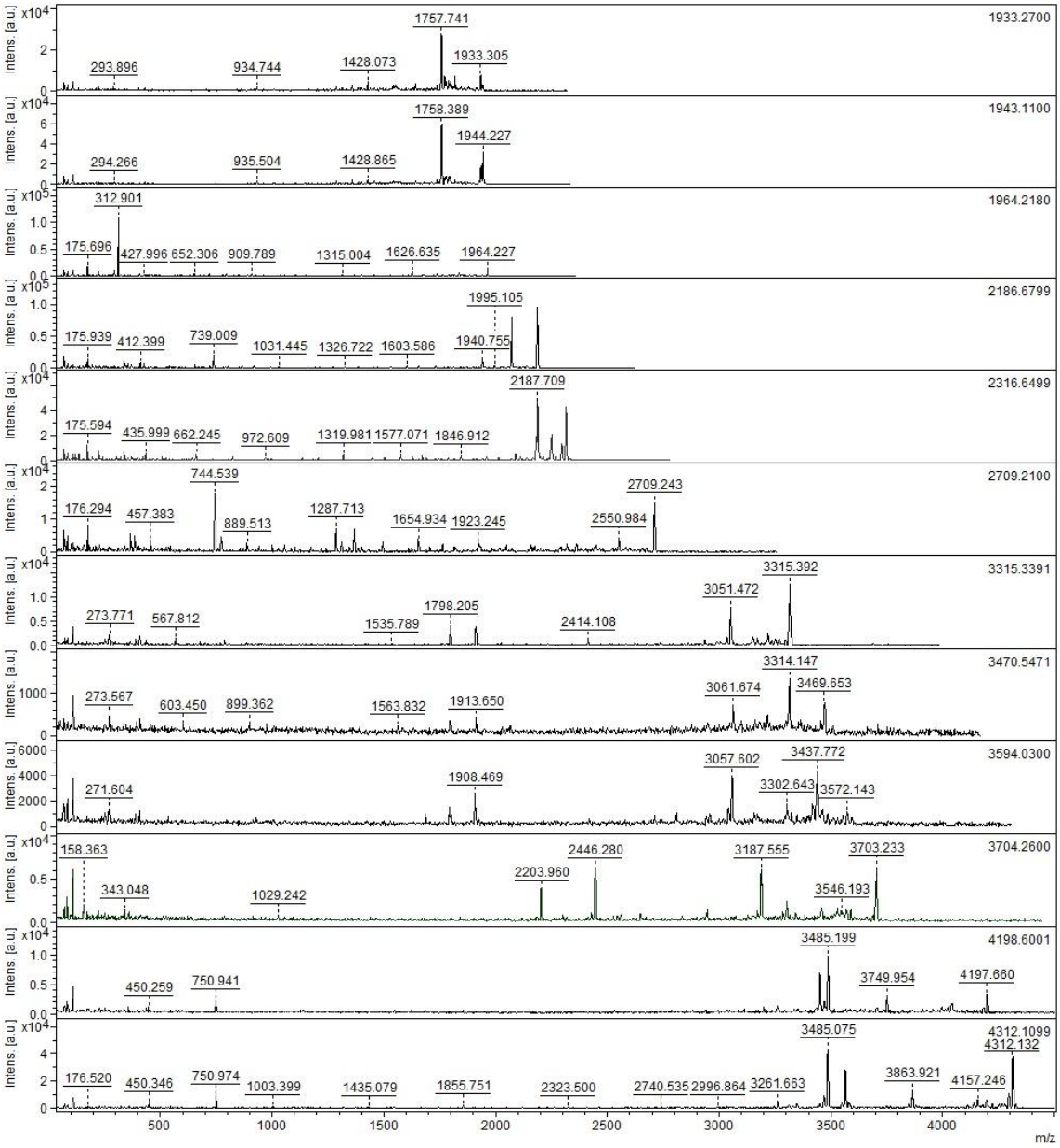

Figure 39c: Mass Spectra of LIFTs Performed on Venom Fractions

APPENDIX 2:

Table 6: Database Query Returns with Variable Search Parameters

Cutoff	Frxn	Mol. Wt	Protein/protein family	Score
50kT	14	23534	HT-2 (Ruberlysin)	67
30k	11	30075	UbiE/COQ5 methyltransferase	57
30k	13	7570	Putative Activator BmCa-1 precursor (Calcium channel toxin Ca1) - Manchurian Sc	49
50kT	21	10612	B0046 protein (fragment)	48
10k	4	8499	Mu-Conotoxin SIIIA precursor - Striated cone	46
30k	14	7570	Toxin BmCa-1 precursor (Calcium channel toxin BmCa1) - Manchurian Scorpion	44
30k	17	7570	Toxin BmCa-1 precursor (Calcium channel toxin BmCa1) - Manchurian Scorpion	42
50kT	13	2868	Dermaseptin-2	39
10k	21	52957	Glutamate-gated chloride channel precursor (Drosophila melanogaster)	39
30k	15	7570	Toxin BmCa-1 precursor (Calcium channel toxin BmCa1) - Manchurian Scorpion	38
30k	9	50479	Endothelin B receptor precursor (Bovine)	38
10k	3	7121	RE27904p (CG32276-PA, isoform A) (Cg32276, isoform b) - Drosophila melanogast	38
30k	15	8499	Mu-Conotoxin SIIIA precursor - Striated cone	37
10k	14	21596	HAM1 protein homolog - Staphylococcus epidermidis	35
10k	21	22645	MotA/TolQ/ExbB proton channel precursor (ATCC43961)	35
50kT	3	32534	HT-2 (Ruberlysin)	34
50kB	15	4692	ORF40f (Pinus koraiensis)	34
50kB	4	7429	PLA2, superbin A	32
30k	18	29544	Salivary antigen-5 related protein AG5-4 (Forest day mosquito)	32
50kT	17	6306	Insulin-like Growth Factor (Pig)	30
30k	21	8355	theta defensin 1b precursor	29
50kB	11	4381	Potassium channel toxin alpha-KTx1.4 (Limbatotoxin) (Scorpion)	28
10k	8	8382	Hypothetical protein - Prochlorococcus marinus (strain MIT 9312)	28
10k	5	8655	theta defensin 1b precursor	28
50kT	14	5875	Defensin - Brown Bumblebee	26
50kB	13	38755	Tumor necrosis factor receptor superfamily member 6 precursor	26
50kB	4	87429	Integrin beta-8 precursor	26
30k	16	7570	Toxin BmCa-1 precursor (Calcium channel toxin BmCa1) - Manchurian Scorpion	25
30k	16	8499	Mu-Conotoxin SIIIA precursor - Striated cone	25
50kB	13	8174	Brevinin-2GHc precursor	24
50kB	3	3227	Disintegrin (Fragment) - Agkistrodon contortrix	21
10k	8	2445	Mu-Conotoxin KIIIA - Kinoshita's cone	21
10k	13	7774	Nitrite reductase apoprotein (fragment) - Barley	21
30k	8	3227	Disintegrin (Fragment) - Agkistrodon contortrix	20
50kT	8	2863	Ponericin-W3 (Ponerine Ant)	19
50kB	3	4122	Toxin SGTx1 - Scodra griseipes	19
10k	16	8499	Mu-Conotoxin SIIIA precursor - Striated cone	19
50kB	11	1396	Tremerogen A-I	18
30k	4	4388	Delta-palutoxin IT3 (Spider)	18
30k	3	3227	Disintegrin (Fragment) - Agkistrodon contortrix	18
10k	11	1761	Fibrinogen alpha chain	18
50kT	11	1761	Fibrinogen alpha chain	17
50kB	21	23985	Interleukin-6 precursor	17
10k	13	5358	Diuretic peptide (House cricket)	17
50kB	9	1646	Alpha-Conotoxin Regle	16
30k	8	14051	PLA2 (Gaboon viper)	15
30k	3	14051	PLA2 (Gaboon viper)	13

APPENDIX 3: MALDI-TOF Mass Data Derived by SNAP Algorithm

10K								
3	4	5	8	11	13	14	16	21
171.723	121.729	101.774	112.559	121.735	121.731	121.736	206.8	121.73
206.804	206.797	121.745	114.566	206.809	206.801	145.732	223.81	143.734
224.833	224.823	145.758	121.733	223.817	223.81	171.74	224.827	206.806
262.808	316.241	171.755	136.59	224.837	224.828	189.766	387.021	224.833
316.222	321.852	172.806	206.811	387.04	246.827	206.804	431.04	246.842
378.941	378.968	182.226	224.839	417.043	287.019	211.768	449.06	262.836
487.037	387.023	189.798	246.839	431.067	431.038	223.813	471.047	290.849
514.251	487.032	190.805	262.829	449.087	449.053	224.831	487.012	306.85
528.265	496.985	191.828	284.835	471.066	471.052	246.829	498.233	316.284
536.26	498.219	211.797	300.822	487.034	487.006	290.844	500.195	321.856
550.285	499.205	277.898	306.855	514.242	514.113	316.26	506.238	383.989
568.274	500.139	334.971	316.272	524.23	644.095	321.824	509.021	387.03
650.206	502.175	336.994	321.85	536.25	650.109	334.945	514.134	431.048
	514.3252	378.992	383.981	550.246	656.128	378.974	514.255	437.077
	528.284	494.389	387.039	550.702	666.086	387.025	524.275	442.011
	536.266	514.222	431.061	568.0255	689.32	431.044	536.272	442.997
	550.284	524.127	443.008	644.073	702.044	449.061	550.685	449.07
	552.252	524.241	449.079	650.108	705.0553	471.052	552.267	453.054
	566.271	536.25	458.933	666.084	708.061	487.021	568.285	454.993
	568.259	550.264	469.013	689.0315	855.182	494.407	608.393	471.054
	587.268	568.137	471.042	702.061	861.179	498.221	644.117	487.038
	608.377	568.257	487.032	705.501	1066.232	514.246	650.134	493.051
	644.207	608.37	509.035	825.187	1173.401	524.096	665.348	498.177
	711.168	628.114	514.269	855.17		524.24	666.109	506.161
	749.126	644.083	524.27	877.177		528.275	679.968	508.181
	833.326	650.102	525.018			536.254	689.333	509.034
	855.301	656.11	528.289			550.276	702.057	514.199
	1060.401	666.077	536.28			568.112	705.546	525.196
	1167.506	679.906	550.286			568.26	711.141	526.223
		689.325	552.259			583.336	718.145	528.226
		702.02	568.299			623.285	749.109	536.198
		705.566	604.393			637.306	855.193	550.2
		708.068	644.105			644.201	861.207	568.212
		718.126	650.129			650.214	877.166	650.137
		855.153	666.091			666.196		656.156
		861.165	679.956			670.392		666.15
		1066.19	702.072			689.462		711.168
		1173.33	711.141			702.197		749.136
			718.193			711.149		864.283
			749.132			855.303		
			855.179			861.322		
			1060.208			1066.357		

30K											
3	4	8	9	11	13	14	15	16	17	18	21
644.082	623.254	644.067	121.749	612.295	121.74	121.735	121.738	121.729	121.738	644.158	608.327
650.094	644.105	650.098	122.724	623.271	171.757	145.74	136.759	206.803	206.812	650.128	644.077
679.0856	650.137	702.03	145.762	637.296	189.787	171.748	206.822	223.813	224.84	656.121	650.11
702.023	702.106	855.143	171.767	650.117	206.817	206.814	223.833	224.829	316.338	666.132	666.076
855.153	825.349	1933.498	172.233	1791.153	211.789	224.842	224.852	246.832	321.866	689.341	689.341
1060.171	841.318		172.823		223.828	316.295	316.275	316.215	387.043	702.074	702.012
1933.4	855.2		189.807		224.846	334.964	321.904	321.861	414.035	855.251	705.594
	1933.38		190.808		316.277	368.285	372.0811	387.035	417.036	861.197	707.997
			191.838		321.835	378.981	387.064	431.053	431.058	1791.241	842.61
			206.815		334.979	381.17	431.9	444.61	449.078	1933.385	855.172
			211.804		379.014	387.043	449.112	449.064	471.068		861.183
			224.841		387.053	414.037	471.11	471.057	487.061		1066.233
			227.785		431.072	431.061	487.091	487.02	494.403		1078.831
			246.846		442.986	449.082	497.123	494.413	497.023		1100.826
			262.839		449.092	471.064	498.266	497.087	498.275		1173.392
			277.909		471.074	487.054	500.224	498.224	506.223		1933.445
			290.785		487.05	497.183	502.234	499.259	514.148		
			316.263		497.166	498.247	506.208	500.195	514.301		
			321.832		498.293	506.274	508.224	502.23	518.188		
			334.995		506.262	508.234	509.104	506.211	524.263		
			379.029		508.23	509.054	510.233	514.129	526.272		
			487.065		509.045	514.135	514.293	514.277	528.332		
			497.201		514.144	514.298	520.27	524.223	536.303		
			498.288		514.305	522.533	522.183	528.26	550.325		
			506.222		524.296	524.321	524.278	536.229	550.583		
			508.239		528.334	525.036	528.33	550.253	568.297		
			514.303		536.298	526.279	536.299	558.251	608.42		
			524.157		547.186	528.317	550.326	566.267	644.242		
			524.305		550.3	536.32	552.238	568.242	650.271		
			528.336		550.617	550.334	568.306	587.333	666.183		
			536.315		550.724	550.585	587.343	644.177	702.139		
			550.608		568.175	568.341	623.345	650.181	855.394		
			550.697		568.324	644.285	644.224	656.252	861.401		
			568.167		644.241	650.291	650.263	689.403			
			568.32		650.273	689.438	702.176	702.119			
			644.262		656.201	702.392	711.244	763.347			
			650.212		689.433	749.179	749.214	855.268			
			702.188		702.327	855.423	855.276	861.273			
			855.378		711.178	861.312		1066.33			
			1046.998		749.159						
					855.389						
					861.416						

50Kb						
3	4	9	11	13	15	21
644.087	608.318	608.389	606.123	644.129	650.096	111.684
702.008	644.061	644.095	608.312	650.141	656.111	121.725
855.164	650.156	650.102	644.098	666.119	666.077	129.658
1933.498	702.075	666.079	650.117	689.35	672.081	143.763
	711.337	702.011	666.091	702.078	682.05	155.722
	749.328	718.116	679.89	708.114	689.308	158.673
	855.216	855.167	701.996	832.443	695.377	159.754
	1680.162	1060.22	718.073	855.213	702.014	171.71
	1964.336	1167.289	833.218	861.232	705.472	172.61
	3315.339		855.183	1933.498	708.011	174.736
	3710.73		871.168		721.62	186.752
	4310.403		1060.231		724.058	187.752
			1933.438		861.172	201.769
					877.151	202.8
					893.123	203.771
						206.808
						215.784
						216.79
						217.794
						218.809
						224.823
						228.823
						230.787
						246.84
						262.838
						268
						268.837
						290.865
						306.854
						316.251
						321.821
						383.981
						442.986
						471.071
						487.047
						493.08
						494.383
						498.182
						509.029
						514.232
						524.231
						528.258
						536.235
						550.256
						550.691
						568.249
						608.153
						650.061
						656.08
						666.036
						689.267
						695.303
						701.987
						705.427
						708.047
						711.158
						749.123
						828.635
						855.264
						861.132

50Kt						
3	8	11	13	14	16	21
1246.65	644.097	608.387	643.968	650.046	608.37	644.123
1387.789	650.126	644.121	650.066	689.244	644.119	650.134
1585.901	702.018	650.139	689.273	861.117	650.152	659.376
1964.103	855.183	656.154	861.134	1192.586	656.152	666.109
	1680.099	666.119	1246.689	1246.7	666.134	689.342
		689.344	1943.168	1585.914	689.379	702.045
		702.025		1679.996	702.065	775.57
		705.539		1764.057	705.525	855.2
		708.039		1964.203	708.098	861.204
		711.379			855.248	1249.902
		749.358			861.266	1934.42
		825.24			877.247	
		855.218				
		861.226				
		1066.263				

APPENDIX 4: Theoretical Digests of Known RDB Proteins, with Zero Missed Cleavages

Chain Snake venom metalloproteinase HT-1

mass	position	peptide sequence
4816.0094	94-135	NGQPCLNNFGYCYNGNCPIL YHQCYALFGSNVYEAEDSCF ER
2962.3630	1-28	LGTDIISPPVCGNELLEVGE ECDCGFPR
2516.9421	71-93	SECDIAESCTGQSADCPMDD FHR
1897.7336	42-58	LHSWVECESGECCGQCK
1424.5933	203-216	VCSNGHCVDVASAY
1308.6113	59-70	FTSAGNECRPAR
1206.5021	180-189	TFNSNEDDHK
1133.4528	169-179	DNSPGPNDSCK
1056.3795	32-41	DPCCDATTCK
971.4866	153-161	IPCAPEDVK
900.3152	139-146	GDDDGYCR
874.4702	190-197	EMVLPGTK
576.2624	148-152	ENGEK
526.2694	165-168	LYCK
493.2075	198-202	CADGK
392.1711	29-31	NCR
389.2143	136-138	NQK
335.1496	162-164	CGR
147.1128	147-147	K

Chain C-type Lectin CRL

mass	position	peptide sequence
3270.5564	34-61	YKPGCHLASFHLYGESLEIA EYISDYHK
1880.8492	1-16	NNCPLDWLPMNGLCYK
1501.7355	104-116	EFCVELVSLSGYR
1430.7062	62-73	GQDNVWIGLWDK
1287.5132	23-32	TWEDAEMFCR
1255.5776	85-94	SCIDYLNWNK
1241.5221	76-84	DFSWEWTDR
1221.5568	117-126	LWNDQVCESK
927.4063	127-134	DAFLCQCK
901.4162	95-101	NQPDHYK
762.4508	17-22	IFNQLK
261.1557	102-103	NK
166.0862	135-135	F
147.1128	33-33	K
147.1128	74-74	K
147.1128	75-75	K

Chain Disintegrin rubistatin

mass	position	peptide sequence
1856.7329	11-27	MRPGSQCAEGLCCDQCR
1467.5838	43-56	NDDTCTGLSADCPR
1025.3849	1-10	NPCCDAATCK
706.3552	37-42	VSMVDR
535.2657	32-36	GTVCR
523.2511	57-61	NGLYG
425.2217	28-30	FMK
147.1128	31-31	K

Chain Rubelase

mass	position	peptide sequence
3326.6806	121-151	NSVGLIQDHSPINLLMGVTM AHELGHNLGMK
2560.3657	92-114	HDNAQLLTAIVLDDYTLGLA YLK
2482.2347	51-72	VSLTDLEIWSDQDFITVQSS AK
1981.0501	1-17	QNLPQSYIELVVVADHR
1706.8934	189-202	FLDQYKPQCILNKP
1679.8540	33-45	VHEIVNFINEFYR
1528.8086	160-174	GASLCIMRPGLTPGR
1192.4939	175-184	SYEFSDASMR
1159.5854	73-82	NTLHSFGEVR
1095.5429	22-30	YNSDLNTIR
730.3123	115-120	SMCHPR
602.3620	46-50	SLNIR
601.2980	185-188	YYQK
556.2622	18-21	MFMK
506.2391	156-159	DCLR
456.2201	152-155	HDGK
446.2973	84-87	SVLK
289.1619	88-89	NR
276.1666	31-32	TR
175.1189	91-91	R
147.1128	83-83	K
147.1128	90-90	K

Chain Snake venom metalloproteinase HT-2

mass	position	peptide sequence
3764.8305	121-155	NSVGLIQDHSPINLLMGVTM AHELGHNLGMEHDGK
3257.6081	92-120	HDNAQLLTAIVLDDYTLGLA YLNSMCHPR
2482.2347	51-72	VSLTDLEIWSDQDFITVQSS AK
1981.0501	1-17	QNLPQSYIELVVVADHR
1706.8934	189-202	FLDQYKPQCILNKP
1679.8540	33-45	VHEIVNFINEFYR
1528.8086	160-174	GASLCIMRPGLTPGR
1246.5963	73-82	NTLHSFGEWR
1192.4939	175-184	SYEFSDASMR
1095.5429	22-30	YNSDLNTIR
701.4304	84-89	SVLLNR
602.3620	46-50	SLNIR
601.2980	185-188	YYQK
556.2622	18-21	MFMK
506.2391	156-159	DCLR
276.1666	31-32	TR
175.1189	91-91	R
147.1128	83-83	K
147.1128	90-90	K

VI. REFERENCES

Albers B, Johnson A, Lewis A. Molecular Biology of the Cell. 4 ed. New York: Garland Science; 2002.

Altschul SF, Gish W, Miller W, Myers EW, Lipman DJ. Basic local alignment search tool. J Mol Biol 1990;215(3):403-410.

Babu M, Diegelmann R, Oliver N. Fibronectin is overproduced by keloid fibroblasts during abnormal wound healing. Mol Cell Biol 1989;9(4):1642-1650.

Babu M, Diegelmann R, Oliver N. Keloid fibroblasts exhibit an altered response to TGF-beta. J Invest Dermatol 1992;99(5):650-655.

Bang RL, Al-Bader AL, Sharma PN, Mattapallil AB, Behbehani AI, Dashti H. Trace elements content in serum, normal skin, and scar tissues of keloid and normal scar patients. Journal of Trace Elements in Experimental Medicine 2002;15(1):57-66.

Bao P, Kodra A, Tomic-Canic M, Golinko MS, Ehrlich HP, Brem H. The role of vascular endothelial growth factor in wound healing. J Surg Res 2009;153(2):347-358.

Barczyk M, Carracedo S, Gullberg D. Integrins. Cell Tissue Res 2010;339(1):269-280.

Bhatia A, Prakash S. Topical phenytoin for wound healing. Dermatol Online J 2004;10(1):5.

Bledzka K, Smyth SS, Plow EF. Integrin alphaIIbbeta3: from discovery to efficacious therapeutic target. Circ Res 2013;112(8):1189-1200.

Bock O, Schmid-Ott G, Malewski P, Mrowietz U. Quality of life of patients with keloid and hypertrophic scarring. Arch Dermatol Res 2006;297(10):433-438.

Bran GM, Sommer UJ, Goessler UR, Hormann K, Riedel F, Sadick H. TGF-ss1 antisense impacts the SMAD signalling system in fibroblasts from keloid scars. Anticancer Res 2010;30(9):3459-3463.

Branton MH, Kopp JB. TGF-beta and fibrosis. Microbes Infect 1999;1(15):1349-1365.

Brinkerhoff CJ, Linderman JJ. Integrin dimerization and ligand organization: key components in integrin clustering for cell adhesion. Tissue Eng 2005;11(5-6):865-876.

Broughton G, Rohrich JR. Wounds and Scars. Selected Readings in Plastic Surgery 2005;10(7).

Broughton G, Janis JE, Attinger CE. The basic science of wound healing. Plast Reconstr Surg 2006;117(7 Suppl):12S-34S.

Carey CM, Bueno R, Gutierrez DA et al. Recombinant rubistatin (r-Rub), an MVD disintegrin, inhibits cell migration and proliferation, and is a strong apoptotic inducer of the human melanoma cell line SK-Mel-28. Toxicon 2012;59(2):241-248.

Chau CH, Clavijo CA, Deng HT et al. Etk/Bmx mediates expression of stress-induced adaptive genes VEGF, PAI-1, and iNOS via multiple signaling cascades in different cell systems. Am J Physiol Cell Physiol 2005;289(2):C444-C454.

Chen L, Tredget EE, Wu PY, Wu Y. Paracrine factors of mesenchymal stem cells recruit macrophages and endothelial lineage cells and enhance wound healing. PLoS One 2008;3(4):e1886.

Chipev CC, Simman R, Hatch G, Katz AE, Siegel DM, Simon M. Myofibroblast phenotype and apoptosis in keloid and palmar fibroblasts in vitro. Cell Death Differ 2000;7(2):166-176.

Chung S, Nakashima M, Zembutsu H, Nakamura Y. Possible involvement of NEDD4 in keloid formation; its critical role in fibroblast proliferation and collagen production. Proc Jpn Acad Ser B Phys Biol Sci 2011;87(8):563-573.

Daopin S, Piez KA, Ogawa Y, Davies DR. Crystal structure of transforming growth factor-beta 2: an unusual fold for the superfamily. Science 1992;257(5068):369-373.

Datubo-Brown DD, Blight A. Inhibition of human fibroblast growthin vitro by a snake oil. British Journal of Plastic Surgery 1990;43(2):183-186.

Dawes KE, Cambrey AD, Campa JS et al. Changes in collagen metabolism in response to endothelin-1: evidence for fibroblast heterogeneity. Int J Biochem Cell Biol 1996;28(2):229-238.

De FB, Ciarmiello LF, Mondola P et al. Differential p63 and p53 expression in human keloid fibroblasts and hypertrophic scar fibroblasts. DNA Cell Biol 2007;26(8):541-547.

Demidova-Rice TN, Hamblin MR, Herman IM. Acute and impaired wound healing: pathophysiology and current methods for drug delivery, part 1: normal and chronic wounds: biology, causes, and approaches to care. Adv Skin Wound Care 2012;25(7):304-314.

Dhananjaya BL, CJ DS. An overview on nucleases (DNase, RNase, and phosphodiesterase) in snake venoms. Biochemistry (Mosc) 2010;75(1):1-6.

Diegelmann RF, Evans MC. Wound healing: an overview of acute, fibrotic and delayed healing. Front Biosci 2004;9:283-289.

Dutertre S, Lewis RJ. Use of venom peptides to probe ion channel structure and function. J Biol Chem 2010;285(18):13315-13320.

Ellis I, Grey AM, Schor AM, Schor SL. Antagonistic effects of TGF-beta 1 and MSF on fibroblast migration and hyaluronic acid synthesis. Possible implications for dermal wound healing. J Cell Sci 1992;102 (Pt 3):447-456.

Ellis R. van Gieson Staining Protocol. 2013. 11-10-2013.

Ref Type: Online Source

English RS, Shenefelt PD. Keloids and hypertrophic scars. Dermatol Surg 1999;25(8):631-638.

Frank S, Hubner G, Breier G, Longaker MT, Greenhalgh DG, Werner S. Regulation of vascular endothelial growth factor expression in cultured keratinocytes. Implications for normal and impaired wound healing. J Biol Chem 1995;270(21):12607-12613.

Frisch SM, Screaton RA. Anoikis mechanisms. Curr Opin Cell Biol 2001;13(5):555-562.

Fujiwara M, Muragaki Y, Ooshima A. Keloid-derived fibroblasts show increased secretion of factors involved in collagen turnover and depend on matrix metalloproteinase for migration. Br J Dermatol 2005;153(2):295-300.

Furtado F, Hochman B, Ferrara SF et al. What factors affect the quality of life of patients with keloids? Rev Assoc Med Bras 2009;55(6):700-704.

Gauglitz GG, Korting HC, Pavicic T, Ruzicka T, Jeschke MG. Hypertrophic scarring and keloids: pathomechanisms and current and emerging treatment strategies. Mol Med 2011;17(1-2):113-125.

Gosain A, DiPietro LA. Aging and wound healing. World J Surg 2004;28(3):321-326.

Hamako J, Suzuki Y, Hayashi N et al. Amino acid sequence and characterization of C-type lectin purified from the snake venom of Crotalus ruber. Comp Biochem Physiol B Biochem Mol Biol 2007;146(3):299-306.

Hao Z, Liu M, Counsell C, Wardlaw JM, Lin S, Zhao X. Fibrinogen depleting agents for acute ischaemic stroke. Cochrane Database Syst Rev 2012;3:CD000091.

Hart PJ, Deep S, Taylor AB, Shu Z, Hinck CS, Hinck AP. Crystal structure of the human TbetaR2 ectodomain--TGF-beta3 complex. Nat Struct Biol 2002;9(3):203-208.

Harvey AL. Chapter 62 - Snake Peptides. In: Kastin AJ, editor. Handbook of Biologically Active Peptides (Second Edition).Boston: Academic Press; 2013. 451-460.

Hoffmann A, Hoying JL, Newman M, Simman R. Role of Hyaluronic Acid Treatment in the Prevention of-áKeloid Scarring. Journal of the American College of Clinical Wound Specialists 2012;4(2):23-31.

Hoying JL. The role of hyaluronic acid treatment in the preventation of keloid formation Wright State University; 2006.

Huang C, Ogawa R. Roles of lipid metabolism in keloid development. Lipids Health Dis 2013;12:60.

Hunasgi S, Koneru A, Vanishree M, Shamala R. Keloid: A case report and review of pathophysiology and differences between keloid and hypertrophic scars. J Oral Maxillofac Pathol 2013;17(1):116-120.

Imaizumi R, Akasaka Y, Inomata N et al. Promoted activation of matrix metalloproteinase (MMP)-2 in keloid fibroblasts and increased expression of MMP-2 in collagen bundle regions: implications for mechanisms of keloid progression. Histopathology 2009;54(6):722-730.

Inui S, Shono F, Nakajima T, Hosokawa K, Itami S. Identification and characterization of cartilage oligomeric matrix protein as a novel pathogenic factor in keloids. Am J Pathol 2011;179(4):1951-1960.

Jain D, Kumar S. Snake venom: a potent anticancer agent. Asian Pac J Cancer Prev 2012;13(10):4855-4860.

Jokinen J, Dadu E, Nykvist P et al. Integrin-mediated cell adhesion to type I collagen fibrils. J Biol Chem 2004;279(30):31956-31963.

Juckett G, Hartman-Adams H. Management of keloids and hypertrophic scars. Am Fam Physician 2009;80(3):253-260.

Kanehisa M, Goto S. KEGG: kyoto encyclopedia of genes and genomes. Nucleic Acids Res 2000;28(1):27-30.

Kanehisa M, Goto S, Sato Y, Kawashima M, Furumichi M, Tanabe M. Data, information, knowledge and principle: back to metabolism in KEGG. Nucleic Acids Res 2013.

Kang N, Sivakumar B, Sanders R, Nduka C, Gault D. Intra-lesional injections of collagenase are ineffective in the treatment of keloid and hypertrophic scars. J Plast Reconstr Aesthet Surg 2006;59(7):693-699.

Kini RM, Gowda TV. Studies on snake venom enzymes: Part I. Purification of ATPase, a toxic component of Naja naja venom & its inhibition by potassium gymnemate. Indian J Biochem Biophys 1982;19(2):152-154.

Kischer CW. The microvessels in hypertrophic scars, keloids and related lesions: a review. J Submicrosc Cytol Pathol 1992;24(2):281-296.

Kishibe M, Bando Y, Tanaka T, Ishida-Yamamoto A, Iizuka H, Yoshida S. Kallikrein-related peptidase 8-dependent skin wound healing is associated with upregulation of kallikrein-related peptidase 6 and PAR2. J Invest Dermatol 2012;132(6):1717-1724.

Komori Y, Sakai K, Masuda K, Nikai AT. Isolation and biochemical characterization of rubelase, a non-hemorrhagic elastase from Crotalus ruber ruber (Red Rattlesnake) venom. Toxins (Basel) 2011;3(7):900-910.

Kurozumi K, Ichikawa T, Onishi M, Fujii K, Date I. Cilengitide treatment for malignant glioma: current status and future direction. Neurol Med Chir (Tokyo) 2012;52(8):539-547.

Leung A, Crombleholme TM, Keswani SG. Fetal wound healing: implications for minimal scar formation. Curr Opin Pediatr 2012;24(3):371-378.

Li WY, Chong SS, Huang EY, Tuan TL. Plasminogen activator/plasmin system: a major player in wound healing? Wound Repair Regen 2003;11(4):239-247.

Lim IJ, Phan TT, Tan EK et al. Synchronous activation of ERK and phosphatidylinositol 3-kinase pathways is required for collagen and extracellular matrix production in keloids. J Biol Chem 2003;278(42):40851-40858.

Louw L. Keloids in rural black South Africans. Part 3: a lipid model for the prevention and treatment of keloid formations. Prostaglandins, Leukotrienes and Essential Fatty Acids 2000;63(5):255-262.

Louw L. The keloid phenomenon: Progress toward a solution. Clin Anat 2007;20(1):3-14.

Lowe GD, Dunlop DJ, Lawson DH et al. Double-blind controlled clinical trial of ancrod for ischemic rest pain of the leg. Angiology 1982;33(1):46-50.

Lu F, Gao J, Ogawa R, Hyakusoku H, Ou C. Biological differences between fibroblasts derived from peripheral and central areas of keloid tissues. Plast Reconstr Surg 2007;120(3):625-630.

Mackessy SP. Fractionation of red diamond rattlesnake (Crotalus ruber ruber) venom: protease, phosphodiesterase, L-amino acid oxidase activities and effects of metal ions and inhibitors on protease activity. Toxicon 1985;23(2):337-340.

Mackessy SP. Handbook of venoms and toxins of reptiles. CRC Press; 2009.

Marangoni FA, Ponce-Soto LA, Marangoni S, Landucci EC. Unmasking snake venom of Bothrops leucurus: purification and pharmacological and structural characterization of new PLA2 Bleu TX-III. Biomed Res Int 2013;2013:941467.

Markland FS, Swenson S. Fibrolase: trials and tribulations. Toxins (Basel) 2010;2(4):793-808.

Marneros AG, Norris JE, Watanabe S, Reichenberger E, Olsen BR. Genome scans provide evidence for keloid susceptibility loci on chromosomes 2q23 and 7p11. J Invest Dermatol 2004;122(5):1126-1132.

Martin P. Wound healing--aiming for perfect skin regeneration. Science 1997;276(5309):75-81.

Masaki T. The discovery of endothelins. Cardiovascular Research 1998;39(3):530-533.

Mayer RJ, Marshall LA. New insights on mammalian phospholipase A2(s); comparison of arachidonoyl-selective and -nonselective enzymes. FASEB J 1993;7(2):339-348.

Meyer LJ, Russell SB, Russell JD et al. Reduced hyaluronan in keloid tissue and cultured keloid fibroblasts. J Invest Dermatol 2000;114(5):953-959.

Momic T, Arlinghaus FT, Arien-Zakay H et al. Pharmacological aspects of Vipera xantina palestinae venom. Toxins (Basel) 2011;3(11):1420-1432.

Morais-Zani K, Tanaka AS, Tanaka-Azevedo AM. Isolation of Bothrops jararaca snake antithrombin from the supernatant of fibrinogen purification. J Biomol Tech 2009;20(5):249-252.

Mori N, Nikai T, Sugihara H, Tu AT. Biochemical characterization of hemorrhagic toxins with fibrinogenase activity isolated from Crotalus ruber ruber venom. Arch Biochem Biophys 1987;253(1):108-121.

Mori N, Nikai T, Sugihara H. Phosphodiesterase from the venom of Crotalus ruber ruber. Int J Biochem 1987;19(2):115-119.

Mosesson MW. Fibrinogen and fibrin structure and functions. J Thromb Haemost 2005;3(8):1894-1904.

Moshref S, Mufti S. Keloid and Hypertrophic Scars: Comparative Histopathological and Immunohistochemical Study. JKAU: Med Sci 2010;17(3):3-22.

Naitoh M, Kubota H, Ikeda M et al. Gene expression in human keloids is altered from dermal to chondrocytic and osteogenic lineage. Genes Cells 2005;10(11):1081-1091.

Nakashima M, Chung S, Takahashi A et al. A genome-wide association study identifies four susceptibility loci for keloid in the Japanese population. Nat Genet 2010;42(9):768-771.

Newman M, Simman R, Krishna S, Grunwald WC Jr, Cool D. Snake Venom as a Putative Treatment for Keloid Scarring. Poster session presented at: Ohio Valley Society of Toxicology Meeting . 9-28-2013. Columbus, OH.

Ref Type: Generic

Nicolas FJ, Hill CS. Attenuation of the TGF-beta-Smad signaling pathway in pancreatic tumor cells confers resistance to TGF-beta-induced growth arrest. Oncogene 2003;22(24):3698-3711.

Nieuwenhuis HK, Akkerman JW, Houdijk WP, Sixma JJ. Human blood platelets showing no response to collagen fail to express surface glycoprotein Ia. Nature 1985;318(6045):470-472.

Oliver N, Babu M, Diegelmann R. Fibronectin gene transcription is enhanced in abnormal wound healing. J Invest Dermatol 1992;99(5):579-586.

Ong CT, Khoo YT, Mukhopadhyay A et al. Comparative proteomic analysis between normal skin and keloid scar. Br J Dermatol 2010;162(6):1302-1315.

Parent JL, Stankova J. Transforming Growth-Factor-Beta Up-Regulates the Gene-Expression of the Human Platelet-Activating-Factor Receptor in Monocytic and B-Cell Lines. Biochemical and Biophysical Research Communications 1993;197(3):1443-1449.

Radis-Baptista G, Kerkis I. Crotamine, a small basic polypeptide myotoxin from rattlesnake venom with cell-penetrating properties. Curr Pharm Des 2011;17(38):4351-4361.

Reilkoff RA, Bucala R, Herzog EL. Fibrocytes: emerging effector cells in chronic inflammation. Nat Rev Immunol 2011;11(6):427-435.

Roberts AB, McCune BK, Sporn MB. TGF-beta: regulation of extracellular matrix. Kidney Int 1992;41(3):557-559.

Roberts AB. Molecular and cell biology of TGF-beta. Miner Electrolyte Metab 1998;24(2-3):111-119.

Romano Di PS, Mangoni A, Zambruno G et al. Adenovirus-mediated VEGF(165) gene transfer enhances wound healing by promoting angiogenesis in CD1 diabetic mice. Gene Ther 2002;9(19):1271-1277.

Russell SB, Russell JD, Trupin KM et al. Epigenetically altered wound healing in keloid fibroblasts. J Invest Dermatol 2010;130(10):2489-2496.

Saed GM, Ladin D, Olson J, Han X, Hou Z, Fivenson D. Analysis of p53 gene mutations in keloids using polymerase chain reaction-based single-strand conformational polymorphism and DNA sequencing. Arch Dermatol 1998;134(8):963-967.

Sauder DN, Kilian PL, McLane JA et al. Interleukin-1 enhances epidermal wound healing. Lymphokine Res 1990;9(4):465-473.

Schomburg I, Chang A, Placzek S et al. BRENDA in 2013: integrated reactions, kinetic data, enzyme function data, improved disease classification: new options and contents in BRENDA. Nucleic Acids Res 2013;41(Database issue):D764-D772.

Seifert O. Keloids: a fibroproliferative disease. 2008.

Shevchenko A, Tomas H, Havlis J, Olsen JV, Mann M. In-gel digestion for mass spectrometric characterization of proteins and proteomes. Nat Protoc 2006;1(6):2856-2860.

Shih B, McGrouther DA, Bayat A. Identification of novel keloid biomarkers through profiling of tissue biopsies versus cell cultures in keloid margin specimens compared to adjacent normal skin. Eplasty 2010;10:e24.

Simman R, Alani H, Williams F. Effect of mitomycin C on keloid fibroblasts: an in vitro study. Ann Plast Surg 2003;50(1):71-76.

Smith CG, Vane JR. The discovery of captopril. FASEB J 2003;17(8):788-789.

Smith JC, Boone BE, Opalenik SR, Williams SM, Russell SB. Gene profiling of keloid fibroblasts shows altered expression in multiple fibrosis-associated pathways. J Invest Dermatol 2008;128(5):1298-1310.

Sporn MB. The Early History of TGF-beta. 2013. 6-2-2013.

Ref Type: Online Source

Straight RC, Glenn JL, Wolt TB, Wolfe MC. North-south regional variation in phospholipase A activity in the venom of Crotalus ruber. Comp Biochem Physiol B 1992;103(3):635-639.

Stroncek JD, Reichert WM. Overview of Wound Healing in Different Tissue Types. 2008.

Szulgit G, Rudolph R, Wandel A, Tenenhaus M, Panos R, Gardner H. Alterations in fibroblast alpha1beta1 integrin collagen receptor expression in keloids and hypertrophic scars. J Invest Dermatol 2002;118(3):409-415.

Takeya H, Onikura A, Nikai T, Sugihara H, Iwanaga S. Primary structure of a hemorrhagic metalloproteinase, HT-2, isolated from the venom of Crotalus ruber ruber. J Biochem 1990;108(5):711-719.

Takeya H, Nishida S, Nishino N et al. Primary structures of platelet aggregation inhibitors (disintegrins) autoproteolytically released from snake venom hemorrhagic metalloproteinases and new fluorogenic peptide substrates for these enzymes. J Biochem 1993;113(4):473-483.

Teixeira CF, Fernandes CM, Zuliani JP, Zamuner SF. Inflammatory effects of snake venom metalloproteinases. Mem Inst Oswaldo Cruz 2005;100 Suppl 1:181-184.

The Uniprot Consortium. Update on activities at the Universal Protein Resource (UniProt) in 2013. Nucleic Acids Res 2013;41(Database issue):D43-D47.

Throckmorton DC, Brogden AP, Min B, Rasmussen H, Kashgarian M. PDGF and TGF-beta mediate collagen production by mesangial cells exposed to advanced glycosylation end products. Kidney Int 1995;48(1):111-117.

Topham MK, Carveth HJ, McIntyre TM, Prescott SM, Zimmerman GA. Human endothelial cells regulate polymorphonuclear leukocyte degranulation. FASEB J 1998;12(9):733-746.

Torii S, Naito M, Tsuruo T. Apoxin I, a novel apoptosis-inducing factor with L-amino acid oxidase activity purified from Western diamondback rattlesnake venom. J Biol Chem 1997;272(14):9539-9542.

Tuan TL, Wu H, Huang EY et al. Increased plasminogen activator inhibitor-1 in keloid fibroblasts may account for their elevated collagen accumulation in fibrin gel cultures. Am J Pathol 2003;162(5):1579-1589.

Ueha S, Shand FH, Matsushima K. Cellular and molecular mechanisms of chronic inflammation-associated organ fibrosis. Front Immunol 2012;3:71.

Vowden P. Hard to heal wounds made easy. Wounds International 2011;2(4).

Walsh BJ, Thornton SC, Penny R, Breit SN. Microplate reader-based quantitation of collagens. Anal Biochem 1992;203(2):187-190.

Wilgus TA, DiPietro LA. Complex Roles for VEGF in Dermal Wound Healing. J Invest Dermatol 2012;132(2):493-494.

Wu MY, Hill CS. Tgf-beta superfamily signaling in embryonic development and homeostasis. Dev Cell 2009;16(3):329-343.

Yang H, Ko HJ, Yang JY et al. Interleukin-1 promotes coagulation, which is necessary for protective immunity in the lung against Streptococcus pneumoniae infection. J Infect Dis 2013;207(1):50-60.

Yen TT, Thao DT, Thuoc TL. An Overview On Keratinocyte Growth Factor - From The Molecular Properties To Clinical Applications. Protein Pept Lett 2013.

Yi D. Tolfenamic Acid Induces Cell Apoptosis and Inhibits Collagen Accumulation in Keloid Fibroblasts Wright State University; 2013.

Zhu F, Wu B, Li P et al. Association study confirmed susceptibility loci with keloid in the Chinese Han population. PLoS One 2013;8(5):e62377.